

ADJOINT CURRENT-BASED APPROACHES TO PROSTATE
BRACHYTHERAPY OPTIMIZATION

BY
JEREMY A. ROBERTS

A THESIS SUBMITTED IN PARTIAL FULFILLMENT
OF THE DISTINCTION OF

HONORS IN RESEARCH
(NUCLEAR ENGINEERING)

DEPARTMENT OF ENGINEERING PHYSICS

UNIVERSITY OF WISCONSIN - MADISON

MADISON, WISCONSIN
MAY 2008

The University of Wisconsin – Madison
Department of Engineering Physics

Candidate for the degree of Bachelor of Science
Nuclear Engineering

Jeremy Alyn Roberts

The undersigned report that a research thesis was completed and defended on May 19, 2008

Thesis title: Adjoint Current-based Approaches to Prostate Brachytherapy Optimization.

*in partial fulfillment of the requirements for the **Undergraduate Honors in Research** designation.*

Committee Members Names

Signature of Committee Members

Henderson, Douglass L.

Thomadsen, Bruce R.

Wilson, Paul P. H.

To coffee, Finnish radio, and all other encouraging things

ABSTRACT

This paper builds on the previous work done at the University of Wisconsin – Madison to employ the adjoint concept of nuclear reactor physics in the so-called greedy heuristic of brachytherapy optimization. Whereas that previous work focused on the adjoint flux, i.e. the adjoint function, this work has included use of the adjoint current to increase the amount of information available in optimizing. Two current-based approaches were developed for 2-D problems, and each was compared to the most recent form of the flux-based methodology. The first method aimed to take a treatment plan from the flux-based greedy heuristic and adjust via application of the current-displacement, or a vector displacement based on a combination of tissue (adjoint) and seed (forward) currents acting as forces on a seed. This method showed promise in improving key urethral and rectal dosimetric quantities. The second method uses the normed current-displacement as the greedy criterion such that seeds are placed in regions of least force. This method, coupled with the dose-update scheme, generated treatment plans with better target irradiation and sparing of the urethra and normal tissues than the flux-based approach. Dose volume histograms and tables of these parameters are given for both approaches. In summary, adjoint current methods were found useful in optimization and further work in 3-D should be performed.

ACKNOWLEDGEMENTS

Some two and a half years ago, ne'er would I have imagined finishing this work, for at the time I had just entered my first class of basic nuclear physics. After bugging Professor Doug Henderson enough about doing some research, he finally agreed; before long, I was being shown images of the multi-dimensional phase-space associated with neutral particle transport. Flabbergasted as I was, I persevered and learned as I went along that someone was smart enough to devise computational methods to deal with all that multi-dimensional stuff; I needed only generate some geometries.

And so it was that the project carried on. Certainly, without the guidance of Professor Henderson, I would not have finished this unique project, so to him first and foremost goes my thanks. Also, I give thanks to Professors Bruce Thomadsen and Paul Wilson who agreed to join my thesis committee rather last minute; their willingness to help is greatly appreciated. Additionally, while I did little work on this project while abroad, Professor Robert Piché of the Tampere University of Technology once demanded of me a mathematical formulation of whatever question it was I asked. I realized at that point I was not using the language I needed for even me to understand well what I was doing, and for that realization, I thank him. During my first summer at ORNL, my mentor John Wagner gave me time to investigate some things related to my work, and I appreciate that support. I would also like to thank Marat Seydaliev for several codes that guided me in reading and analyzing much of the data used throughout my work. Finally, I want to thank the numerous people who have suffered excessively in-depth conversations about this work, while managing the while to nod politely; of them, Sammie deserves particular thanks.

TABLE OF CONTENTS

ABSTRACT	iii
ACKNOWLEDGEMENTS	iv
1 INTRODUCTION	1
1.1 Motivation	1
1.2 Organization of Report	2
2 THEORETICAL FOUNDATIONS	3
2.1 Neutral Particle Transport	3
2.2 The Scalar Flux	7
2.3 The Current Vector	13
2.4 The Adjoint-based Greedy Heuristic	13
2.5 Evaluating Treatment Plans	17
3 DATA GENERATION AND MODELING	22
3.1 DANTSYS: A Neutral Particle Transport Code	22
3.2 Prostate Model: Adjoint Fluxes and Current Generation	24
3.3 Seed Model: Forward Current and Dose Profiles	26
3.4 Implementation in MATLAB	31
4 CURRENT-DISPLACEMENT: A “NUDGE”	34
4.1 Theory	34
4.2 Defining Current-displacement	34
4.3 Results and Discussion	38
5 A NEW GREEDY CRITERION	52
5.1 Theory	52
5.2 Results and Discussion	54
6 CONCLUDING REMARKS	69
A SCALAR FLUX UTILITY	71
B CURRENT VECTOR UTILITY	75
C DANTSYS INPUT EXAMPLE	79
REFERENCES	83

LIST OF FIGURES

2.1	The position and direction variables describing a particle.	4
2.2	Forward transport from a single source in the prostate.	9
2.3	Adjoint transport from a single source in the rectum.	10
3.1	Adjoint functions and ratio for slice 7.	25
3.2	Target Current, Slice 7.	26
3.3	Urethra Current, Slice 7.	27
3.4	Rectum Current, Slice 7.	27
3.5	Normal Current, Slice 7.	28
3.6	Normed current for target and urethra, slice 7.	28
3.7	Dose Profile for 2-D Seed Model.	30
3.8	Comparison of 2-D Model and TG-43 Radial Dose Profile.	31
3.9	Schematic target outline [2].	32
3.10	Binary mask file for target [2].	32
4.1	GY+CD: DVH's for each slice with $f = 1$	41
4.2	GY+CD: Seed placements, $f = 1$	42
4.3	GY+CD: DVH's for each slice with $f = 2$	44
4.4	GY+CD: Seed placements, $f = 2$	45
4.5	GY+CD: DVH's for each slice with $f = 3$	47
4.6	GY+CD: Seed placements, $f = 3$	48
5.1	CD: DVH's for each slice with $f = 1$, with grid.	56
5.2	CD: DVH's for each slice with $f = 1$, with grid.	57
5.3	CD: DVH's for each slice with $f = 2$, with grid.	59
5.4	CD: Seed placements, $f = 2$, with grid.	60
5.5	CD: Seed placements, $f = 1$, without grid.	62
5.6	CD: Seed placements, $f = 1$, without grid.	63
5.7	CD: DVH's for each slice with $f = 2$, without grid.	65
5.8	CD: Seed placements, $f = 2$, without grid.	66

LIST OF TABLES

3.1	ICRP-21 Flux-to-dose Conversion Factors.	29
3.2	Matrix Dimensions and Their Notation.	33
4.1	GY+CD: Evaluation parameters for $f = 1$	40
4.2	GY+CD: Evaluation parameters for $f = 2$	43
4.3	GY+CD: Evaluation parameters for $f = 3$	46
5.1	CD: Evaluation parameters for $f = 1$, with grid.	55
5.2	CD: Evaluation parameters for $f = 2$, with grid.	58
5.3	CD: Evaluation parameters for $f = 1$, without grid.	61
5.4	CD: Evaluation parameters for $f = 2$, without grid.	64

CHAPTER 1

INTRODUCTION

1.1 Motivation

Brachytherapy is an increasingly popular methodology for treatment of prostate and other cancers. From the Greek *brakhus* for near, brachytherapy is radiation treatment applied close to the target of interest. For prostate cancer in particular, interstitial brachytherapy is highly useful. In this procedure, radioactive implants or “seeds” are placed within the cancerous region for some amount of time; here, *permanent implants* are the focus. Typically, these seeds are placed at intervals within needles, which are then inserted into the tumor region by way of the rectum. Frequently, this procedure is done via the assistance of trans-rectal ultrasound imaging.

Optimizing the placement of permanent brachytherapy seeds is a difficult task. Over the past several years, numerous attempts to apply robust optimization techniques to brachytherapy have been met with ample success; however, even as computational power reaches new heights, these optimization routines still require too much time for “on-the-fly” treatment planning. Therefore, methods that provide adequate plans in short periods of time are desired.

Much work has been done at the University of Wisconsin – Madison in applying the adjoint method of reactor physics to brachytherapy optimization. Specifically, the

“greedy heuristic” of Yoo [14] [13] and her predecessor Chaswal [2] has shown to be a highly efficient method that yields good results. However, it was thought by applying further methods from the adjoint theory that better plans could still be found. The present work aims to do exactly this.

1.2 Organization of Report

The rest of this report provides the theory needed for later method development, followed by a discussion of the most recent form of the adjoint flux-based greedy heuristic. Evaluation criteria are provided that are used to compare treatment plans. The report then details the theory and application of the current-displacement technique for adjusting a given seed placement generated by the flux-based approach, providing a comparison and discussion. Next, the theory and application of the normed current-displacement as the “greedy criterion” are provided, as are comparisons to the flux-based approach. Finally, some concluding remarks and a brief discussion of possible future work in current-based methods are provided.

CHAPTER 2

THEORETICAL FOUNDATIONS

2.1 Neutral Particle Transport

For many applications, including brachytherapy, a time-independent treatment of particle interactions is sufficient to determine all dosimetric quantities. The time-independent form of the Boltzmann transport (or simply Boltzmann) equation for non-multiplying (i.e. no fissile material) systems is written

$$[\hat{\Omega} \cdot \vec{\nabla} + \Sigma(\vec{r}, E)]\psi(\vec{r}, \hat{\Omega}, E) = q_{ex}(\vec{r}, \hat{\Omega}, E) + \int dE' \int d\Omega' \Sigma_s(\vec{r}, E' \rightarrow E, \hat{\Omega}' \cdot \hat{\Omega})\psi(\vec{r}, \hat{\Omega}', E') \quad (2.1)$$

if the boundary conditions are also time-independent [9]. For all the work considered in this paper, this latter condition is assumed to hold.

The time-independent Boltzmann transport equation is a six-dimensional linear equation that determines the location, direction, and energy of neutral particles in a medium. As written, the particle's position is defined by \vec{r} , which in Cartesian coordinates simply represents the point (x, y, z) in three-space. Furthermore, the variable $\hat{\Omega}$ can best be defined as the two-component vector comprised of the polar and azimuthal angles θ and ϕ , which define the direction of the particle's movement.

Finally, the particle's energy is simply a scalar quantity, E . Fig. 2.1 presents a basic schematic of these quantities. Surely, the Boltzmann equation is equally adaptable to other coordinate systems; however, for this brief outline, the Cartesian system suffices.

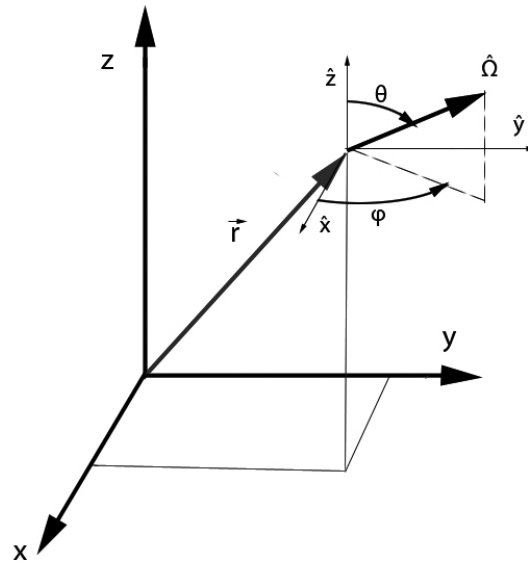


Figure 2.1: The position and direction variables describing a particle.

2.1.1 An Intuitive Formulation

To understand more deeply the meaning of the Boltzmann equation, it serves us well to define some basic quantities so that we might derive the equation in a somewhat intuitive fashion. This discussion does not aim to be rigorous; there are many such treatments available, e.g. [9],[1].

For a given particle population in some medium, we define the *particle density distribution*

$$N(\vec{r}, \hat{\Omega}, E) d^3r d\Omega dE \quad (2.2)$$

to be the expected number of particles within the energy range dE about E , traveling in the cone $d\Omega$ about $\hat{\Omega}$, within the volume d^3r about \vec{r} .

Additionally, turning back to Eq. 2.1, we define our *total macroscopic cross-section*, $\Sigma(\vec{r}, E)$, to be the inverse of the mean free path of a particle of energy E at a point \vec{r} in the medium. Alternatively, it may be defined as the probability per unit path length that the particle will interact via some mechanism.

Now, multiplying N by the velocity v of the particles, we define the *angular flux*,

$$\psi(\vec{r}, \hat{\Omega}, E) = vN(\vec{r}, \hat{\Omega}, E). \quad (2.3)$$

If we multiply ψ (which is in units of particles-distance per time-volume) by the volume $d^3rd\Omega dE$, we note that we have the total distance traveled (by all particles in the volume) per unit time. Multiplying this latter quantity by our total cross-section, we have

$$vN(\vec{r}, \hat{\Omega}, E)d^3rd\Omega dE\Sigma(\vec{r}, E) = \psi(\vec{r}, \hat{\Omega}, E)d^3rd\Omega dE\Sigma(\vec{r}, E) = dR(\vec{r}, \hat{\Omega}, E), \quad (2.4)$$

the total number of interactions per unit time in the differential volume.

Referring again to Eq. 2.1, we define the *scattering cross-section* $\Sigma_s(\vec{r}, E' \rightarrow E, \hat{\Omega}' \cdot \hat{\Omega})$ to be the probability that a particle at \vec{r} of energy E' and traveling in the direction $\hat{\Omega}'$ is scattered into an energy interval dE about E and into a cone $d\Omega$ about $\hat{\Omega}$

2.1.2 The Boltzmann Equation: Term by Term

Knowing these definitions, it is easier for us to see what exactly Eq. 2.1 describes.

Starting with the left hand side, we note two terms. The first of these,

$$\hat{\Omega} \cdot \vec{\nabla} \psi(\vec{r}, \hat{\Omega}, E), \quad (2.5)$$

is known as the *streaming* term, as it represents particles that “stream” or “leak” out of the differential volume [9]. The second term,

$$\Sigma(\vec{r}, E) \psi(\vec{r}, \hat{\Omega}, E), \quad (2.6)$$

represents all particle interactions within the volume that cause particles to enter a new energy or direction; such interactions include collisions and absorption. Note, by defining the *collision* term in this fashion, we imply that any interaction removes a particle from the differential phase-space volume (i.e. $d^3rd\Omega dE$) of interest; this is true, for if a particle does not change energy or direction, it seems impossible to say it interacted!

These two terms, then, appear to be ways by which particles *leave* the given volume element. On the other hand, the terms of the right hand side of Eq. 2.1 describe just the opposite. The first term,

$$q_{ex}(\vec{r}, \hat{\Omega}, E), \quad (2.7)$$

simply represents an external source emitting particles of energy E at \vec{r} and in the

direction $\hat{\Omega}$. The second term,

$$\int dE' \int d\Omega' \Sigma_s(\vec{r}, E' \rightarrow E, \hat{\Omega}' \cdot \hat{\Omega}) \psi(\vec{r}, \hat{\Omega}', E') \quad (2.8)$$

is quite more complicated. However, recalling our definition for ψ , we see the second integral represents the total number of particles of energy E' at \vec{r} that are scattered into the cone $d\Omega$ about $\hat{\Omega}$. The first integral, over energy, gives to us the total number of particles at \vec{r} that are scattered into the cone $d\Omega$ about $\hat{\Omega}$ and into energy interval dE about E ; in essence, this double integral gives to us yet another a source of particles at \vec{r} , going in $\hat{\Omega}$ and of energy E .

Thus, we see the Boltzmann equation is nothing but a balance of particles within a given differential phase-space volume. On the left hand side, what leaves the volume must be equivalent to what enters the volume, denoted by the right hand side. This equality is most evident by noting we are working with the time-independent form, and therefore the derivative of ψ with respect to time, which is just equal to the source terms minus the leakage and collision terms, must be zero; we therefore have the balance as described.

2.2 The Scalar Flux

For calculating reaction rates of interest, e.g. dose rates, it is easiest to use a quantity called the *scalar flux* or simply *flux* that describes the population of particles of energy E at \vec{r} without reference to angle. We define this mathematically as

$$\phi = \int_{4\pi} d\Omega \psi(\vec{r}, \hat{\Omega}, E). \quad (2.9)$$

If we recall Eq. 2.4, we note that the reaction rate integrated over all angles is simply

$$dR(\vec{r}, E) = \int_{4\pi} d\Omega \psi(\vec{r}, \hat{\Omega}, E) d^3 r dE \Sigma(\vec{r}, E) = \phi(\vec{r}, E) d^3 r dE \Sigma(\vec{r}, E). \quad (2.10)$$

This can be integrated over energy and volume to yield

$$R(\vec{r}) = \int_V \int_E \left(\phi(\vec{r}, E) \Sigma(\vec{r}, E) dE d^3 r \right). \quad (2.11)$$

For the purposes of dosimetry, this R is often referred to as the *detector response* if we substitute for Σ in Eq. 2.11 a *detector response function* or rather, a *dose response function*. Such functions are tabulated as *flux-to-dose* conversion factors DF for set intervals of energy. We will discuss these in more detail below.

2.2.1 The Forward Case

The *flux* as defined already refers to the *forward scalar flux*; in other words, it is calculated by *forward* transport, by which particles are emitted from a known source, traverse a medium, and impart their energy along the way. In some cases, particles reach a certain detector of interest. In our case, we are most interested in different organs, specifically the prostate or the neighboring urethra, rectum, and other healthy tissues as the “detector”, whereas radioactive implants will be our *forward source*. This distinction is of paramount importance when we consider the *adjoint* form of the transport equation. Following the pedagogy of Chaswal [2], we show explicitly what is meant by forward transport.

Fig. 2.2 shows a simple two-dimensional slice of a prostate and the sensitive tissues; each is labeled by color. The white dots correspond to the seed locations allowed by the treatment grid and the square regions are denoted voxels. Placing a

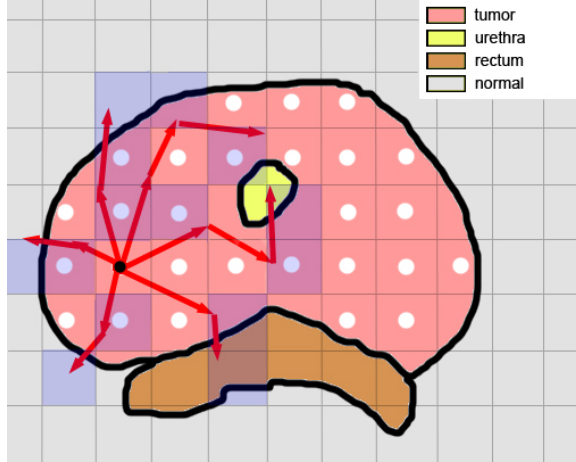


Figure 2.2: Forward transport from a single source in the prostate.

seed at one such location, we track the paths of emitted photons using the red rays and shade the voxels in which particles undergo a collision, i.e. impart energy. For each voxel, the forward flux can be calculated, and thus, we can find for each voxel an associated detector response or dose. Note that in a realistic scenario, the voxels are much smaller than depicted.

2.2.2 The Adjoint Case

A Gedanken Experiment

In addition to the forward case, we can also describe the *adjoint* form of the Boltzmann equation and flux. To preface mathematical definitions, let us first do a “mind” experiment. Let a particular region that was once our detector be a source, say q^+ . Moreover, let this source be equivalent to some desired detector response; in other words, imagine our source particles are “pseudo-particles” representing the desired response. Now, setting the particles in motion, we apply all the same physics, but in *reverse order*. That is to say, our particles spread out while *increasing in energy*.

Some “adjoint” particles, in theory, could never cease to exist, and in fact, might become infinitely energetic; we know better, though, and realize our problem has boundaries past which these particles cannot go. Just as our initial (forward) problem has boundaries from outside which particles cannot *come*, our “adjoint” particles may not *leave*.

The population of “adjoint” particles can be described by the *adjoint flux*, a function of space and energy. The position and energy of an “adjoint” particle along its path is uniquely valuable: its energy and position are the same as a forward particle’s energy and position that would go back on the same path to induce the desired response! We might guess, then, that *the more probable a small region in space is in letting a forward source of some energy achieve a desired response, the more likely it is that adjoint particles emitted from our adjoint source will be found in that same region with that same energy.*

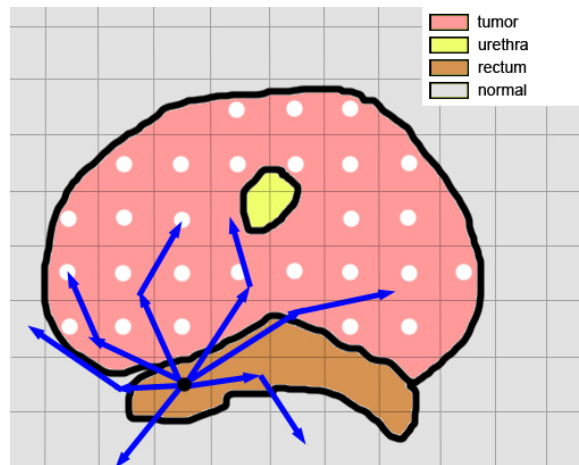


Figure 2.3: Adjoint transport from a single source in the rectum.

As for the forward case, we show explicitly what adjoint transport means. Using the same schematic as Fig. 2.2, Fig. 2.3 depicts a pixel of the rectum as the adjoint source. The adjoint particle, denoted by the blue rays, are emitted and outscatter,

becoming more energetic with each collision. Some of these rays end at the possible forward source locations. For each of these such locations, we can calculate the adjoint flux and subsequently know how important those locations are to the detector response, here rectal dose.

Mathematical Idea

For an operator H , we define the associated adjoint operator H^+ by the relation

$$\langle \psi^+ H \psi \rangle = \langle \psi H^+ \psi^+ \rangle \quad (2.12)$$

where $\langle \cdot \rangle$ denotes integration over all variables [9].

We take the time-independent, nonmultiplying forward transport operator H to be such that

$$\begin{aligned} H\psi &= [\hat{\Omega} \cdot \vec{\nabla} + \Sigma(\vec{r}, E)]\psi(\vec{r}, \hat{\Omega}, E) \\ &\quad - \int dE' \int d\Omega' \Sigma_s(\vec{r}, E' \rightarrow E, \hat{\Omega}' \cdot \hat{\Omega})\psi(\vec{r}, \hat{\Omega}', E'), \end{aligned} \quad (2.13)$$

from which we note

$$H\psi = q_{ex}(\vec{r}, \hat{\Omega}, E) \quad (2.14)$$

is equivalent to Eq. 2.1 [9].

By starting with $\langle \psi^+ H \psi \rangle$ and working toward $\langle \psi H^+ \psi^+ \rangle$, one finds [9] that the adjoint transport operator H^+ may be written

$$\begin{aligned} H^+ \psi^+ &= [-\hat{\Omega} \cdot \vec{\nabla} + \Sigma(\vec{r}, E)]\psi^+(\vec{r}, \hat{\Omega}, E) \\ &\quad - \int dE' \int d\Omega' \Sigma_s(\vec{r}, E \rightarrow E', \hat{\Omega} \cdot \hat{\Omega}')\psi^+(\vec{r}, \hat{\Omega}', E') \end{aligned} \quad (2.15)$$

where ψ^+ is the adjoint angular flux. Furthermore,

$$H^+ \psi^+ = q_{ex}^+(\vec{r}, \hat{\Omega}, E) \quad (2.16)$$

the adjoint source, or detector response. From Lewis and Miller[9], we have an illustrative example to show what the adjoint entails mathematically. Suppose we have a known forward source, q_{ex} , and that we want to find the response of some small detector with cross section Σ_d and of volume V_d centered at \vec{r}_d . The associated reaction rate is simply

$$R = V_d \int dE \Sigma_d(E) \phi(\vec{r}_d, E). \quad (2.17)$$

Our adjoint problem is defined

$$H^+ \psi^+ = \Sigma_d V_d \delta(\vec{r} - \vec{r}_d). \quad (2.18)$$

By multiplying Eq. 2.14 by ψ^+ and integrating over all variables, we have

$$\langle \psi^+ H \psi \rangle = \langle \psi^+ q_{ex} \rangle, \quad (2.19)$$

and if we multiply Eq. 2.18 by ψ and integrate, we have

$$\langle \psi H^+ \psi^+ \rangle = \langle \psi \Sigma_d V_d \delta(\vec{r} - \vec{r}_d) \rangle = R. \quad (2.20)$$

Because the difference of the left hand sides of Eqs. 2.19 and 2.20 is zero by Eq. 2.12, we have

$$R = \langle \psi^+ q_{ex} \rangle. \quad (2.21)$$

Thus, our detector response is simply the adjoint-weighted source distribution. In

other words, the adjoint flux defines the relative importance some component of the forward source has on the detector response. Fortunately, this is the basic idea we got from our mind experiment above!

2.3 The Current Vector

A quantity essential for later chapters is the so-called *current vector* or simply *current*. We saw above the scalar flux is the angular flux integrated over all directions. However, we may want to incorporate directional information into a quantity without it being a function of angle. We do this by defining the forward current,

$$\bar{J}(\vec{r}, E) = \int_{4\pi} d\Omega \hat{\Omega} \psi(\vec{r}, \hat{\Omega}, E) \quad (2.22)$$

and similarly, the adjoint current,

$$\bar{J}^+(\vec{r}, E) = \int_{4\pi} d\Omega \hat{\Omega} \psi^+(\vec{r}, \hat{\Omega}, E). \quad (2.23)$$

These current vectors represents *net* flow of particles—both forward and adjoint—through a differential phase space volume. We will turn to the current again later.

2.4 The Adjoint-based Greedy Heuristic

Much work has been done to employ adjoint fluxes in optimization schemes for brachytherapy optimization. Specifically, at the University of Wisconsin - Madison, a greedy heuristic based on a so-called adjoint ratio was developed [14, 13]. Later work refined the general concept by developing more efficient ways to avoid seed clustering [2] and incorporating directional seeds [2, 4, 3]. We shall take the later work,

namely its *greedy heuristic with dose update*, as the standard by which to compare the methods developed later in this report. For the remainder of this section, we will describe general “greedy” methods, the adjoint function, and the basics of the *greedy heuristic*.

2.4.1 The Adjoint Function

If we have the adjoint flux for a region of interest (ROI), $\phi_{ROI}^+(\vec{r})$, and multiply it by the appropriate constant C_{1S_u} yielding units Gy/S_u, where SS_u (read “source unit”) represents a 0.43 mCi ¹²⁵I seed. Then, by dividing the function by the volume V_{ROI} of the region, we have the so-called *adjoint function*

$$D_{ROI}^+(\vec{r}) = C_{1S_u} \phi_{ROI}^+(\vec{r}) / V_{ROI}. \quad (2.24)$$

This function essentially defines the sensitivity of the ROI’s dose to a 1 S_u seed placed at \vec{r} [14]. It should be noted the definition used here for the adjoint function looks different than the cited literature. This is due simply to the fact that this report shall employ software which calculates the adjoint flux explicitly from which we may find D^+ ; contrarily, the literature employs a method by which the adjoint function is found by using a forward dose kernel (rather than a transport code). More of this will be discussed in Chapter 3.

We note, however, that we often work with several ROI’s. To capture the relative sensitivity of all ROI’s, we define the *adjoint ratio* to be the sum of the adjoint functions for all non-target ROI’s divided by the adjoint function of the target ROI. Mathematically, this is written

$$\rho(\vec{r}) = \frac{w_u D_u^+(\vec{r}) + w_r D_r^+(\vec{r}) + w_n D_n^+(\vec{r})}{D_t^+(\vec{r})} \quad (2.25)$$

where the w 's are weighting factors that define the relative importance of each non-target or *sensitive* tissue [14]. This quantity can roughly be considered a measure of the dose to the target region relative to the overall sparing of these sensitive tissues.

2.4.2 Greedy Methods

Optimization algorithms usually go through steps in sequence, with several choices (i.e. a subproblem) at every step. For many problems, dynamic programming methods, or “true” optimization routines, are quite successful in determining solutions; however, they are also time consuming, so we look for simpler, more efficient methods. One such class of methods are known as *greedy* algorithms. A greedy algorithm chooses at each step the option that best satisfies some *greedy criterion*; in other words, greedy algorithms yield locally optimal solutions, which hopefully together lead to a global solution [5].

2.4.3 Greedy Heuristic with Dose Update

The greedy heuristic for brachytherapy optimization employs a greedy algorithm for generating seed and needle placements that satisfy certain dosimetric requirements. Because we are working in only two dimensions, we will not concern ourselves with the needles used to insert seeds into the treatment region.

For the greedy criterion, the adjoint ratio is employed. Essentially, the algorithm chooses the coordinate with the *lowest* adjoint ratio, which signifies the seed location that has the highest tumor-dose to tissue-sparing value. After the first placement, though, a mechanism must be used by which seed clustering is avoided. For instance, a small volume that contains the lowest ratio coordinate will likely have neighboring locations of relatively low ratio values, one of which might be the next best location

for a seed. However, this would lead to overdosing, which must be avoided.

To accommodate this, the rather complicated *exclusion zone* method of using isodose curves to define the solution space has been suggested [14]. However, a method incorporating the dose distribution has shown to be much simpler and more efficient, which is now described [2].

The dose-based sensitivity at a voxel j is defined

$$S_{dose}(j) = \frac{1}{D_p} \sum_{i=1}^n D(i, j) \quad (2.26)$$

where D_p is the prescribed dose and $D(i, j)$ is the dose to a voxel j from a seed at voxel i . From this, we define a new quantity

$$\rho_d(j) = \rho(j) S_{dose}(j) \quad (2.27)$$

where $\rho(j)$ is the adjoint ratio evaluated at voxel j .

This new metric becomes our greedy criterion. While $\rho(j)$ selects seed positions based solely on their simultaneous impact on tumor dose and tissue sparing, the new metric $\rho_d(j)$ contains this feature along the intrinsic ability to disperse seeds. Using the dose as an update function makes sense, for if the goal is to disperse seeds primarily to limit dose “hot spots”, shaping the overall importance function by the current dose necessarily places the next seed away from zones where such hot spots would develop.

As opposed to the previous dispersion methods (i.e. exclusion zones), by using ρ_p as our criterion, we allow for an uninterrupted addition of seeds [2]. In the exclusion zone method, certain parameters could lead to a null solution space causing the whole algorithm to restart with modified parameter values. This leads to unnecessary com-

putational expense. Because the dose-update mechanism shown here never restricts the solution space, the algorithm can run its course without such restarting. Alg. 1 provides the basic schematic of the greedy method with dose-update.

```

Input: Adjoint currents, seed dose profile, and patient geometry.
Output: Optimized treatment plan.

calculate  $\rho$  ;
sort  $\rho$  in increasing order ;
place first seed at position of  $\min \rho$  ;
it  $\leftarrow 0$ ;
 $D_p = 145$  Gy;
dcov  $\leftarrow 98\%$ ;
dose  $\leftarrow$  finddose(seed locations);
 $V_{100} \leftarrow$  findv100(dose);
while  $V_{100} \leq dcov$  or  $it \leq itmax$  do
|  $it \leftarrow it + 1$ ;
|  $\rho \leftarrow \rho \times dose/D_p$ ;
| sort  $\rho$  in increasing order ;
| place next seed at position of  $\min \rho$  ;
| dose  $\leftarrow$  finddose(seed locations);
end
```

Algorithm 1: Greedy heuristic with dose-update.

2.5 Evaluating Treatment Plans

2.5.1 Background

For any treatment plan devised in some fashion to be evaluated, evaluation criteria that consider all aspects of the problem (e.g. dose to the tumor, dose to other tissues) must be used. Chaswal [2] performs a good review of the current literature and provides a robust set of parameters we shall employ herein. Many of the ideas are summarized elsewhere, e.g. the recommendations of the American Brachytherapy Society [10], and the reports of two AAPM Task Groups [12],[15].

For all plans, dose volume histograms (DVH's) of the target, urethra, rectum and

normal tissues are calculated. In addition, several evaluation parameters are used which we now describe.

2.5.2 Evaluation Parameters

Target Coverage

Perhaps the most important aspect of radiotherapy is ensuring the target is given a sufficient dose. To quantify whether a plan does that, we define three parameters. The first, V_{100} , is the percentage of the target volume that receives a dose greater than or equal to D_p , the prescribed dose. Thus, V_{100} is a direct metric for target coverage.

Similarly, we define V_{150} as the target volume receiving greater than or equal to $1.5D_p$; therefore, V_{150} measures “hot spots” in the target.

Finally, we define D_{90} , which is the minimum dose received by 90% of the target volume. A D_{90} value greater than or equal to D_p is a measure of so-called dose quality. If D_{90} is below the prescribed dose, then the treatment plan is likely insufficient.

Dose Nonuniformity Ratio

In treatment planning, it is highly desirable to have as homogeneous a dose delivery within the target as possible, so as to avoid “hot spots” and unnecessary necrosis. One measure of such homogeneity is the so-called *dose nonuniformity ratio* (DNR), which is defined

$$DNR = \frac{V_h}{V_l} \quad (2.28)$$

where V_h is the volume receiving a dose equal to or greater than some high dose h and V_l is the volume receiving a dose equal to or greater than some low dose l . As

used by Chaswal and others, we set $h = 1.5D_p$ and $l = D_p$, or $DNR = V_{150}/V_{100}$.

We note that since the numerator is a subset of the denominator, i.e. a volume receiving $1.5 D_p$ also receives D_p , $DNR \in (0, 1)$. Moreover, because DNR directly measures the “price paid in terms of excessive dose in order to cover the target adequately”, lower values of DNR are preferred [2].

Conformation Number

To describe how well a dose conforms to the target volume, we define the *conformational number*

$$CN = \frac{V_{t,D_p}}{V_t} \times \frac{V_{t,D_p}}{V_{D_p}} \quad (2.29)$$

where V_{t,D_p} is the target volume receiving at least the prescribed dose D_p , V_t is the total target volume, and V_{D_p} is the total volume receiving at least the prescribed dose.

The first term measures how well the dose covers the volume, while the second measures how well the dose is confined to the target. Since each component lies between zero and one, $CN \in (0, 1)$. Because a greater CN value indicates better dose conformation to the target, we look for treatment plans with high CN values. (Note, 0.72 is average; use this later)

Urethra Dosimetry

Currently, no set parameters for assessing the dosimetry of the urethra have been established. However, a few quantities do serve as helpful metrics.

First, $V_{360,Ur}$ is defined as the volume of urethra tissue receiving a dose equal to or greater than 360 Gy, a level that has been shown to correlate well with urinary morbidity.

Second, $D_{10,Ur}$ is defined as the minimum dose to 10% of the urethral volume; thus, it measures the highest of doses to the urethral volume. Similarly, $D_{90,Ur}$ is defined as the minimum dose to 90% of the urethral volume. Because the urethra is defined by some to be part of the target region (though still not to be overdosed), $D_{90,Ur}$ should be at least equal to D_p while exceeding it as little as possible.

Finally, $V_{125,Ur}$ is defined as the urethral volume receiving $1.25D_p$, which, like V_{150} for the target, measures “hot spots” in the urethra.

Rectum Dosimetry

The standard method of describing the rectum as an entire organ, i.e not just its walls, was employed. Therefore, a number of volumetric indicators are available for comparison. First, $V_{90,re}$ is defined to be the rectal volume receiving a dose greater than or equal to 90 Gy. Apparently, a dose greater than 90 Gy to the rectal wall induces bleeding ulceration. Additionally, $D_{90,re}$ is the minimum dose received by 90% of the rectal volume.

Because the rectum is a sensitive organ, all efforts should be made to ensure a treatment plan has the lowest possible $V_{90,re}$ and $D_{90,re}$ values.

Normal Tissue Dosimetry

For this work, the normal tissue is defined as everything outside the other tissues specified. The single metric used is $D_{90,no}$, the minimum dose received by 90% of the normal tissue volume. Because we try to avoid secondary cancer in non-target tissue, a low value for $D_{90,no}$ is desired.

Number of seeds and needles

Studies have shown the local trauma induced by needles leads to locally reduced doses. Subsequently, in three-dimensional plans, the number of needles should be minimized; however, we do not account for needles here, given we work solely with planar models.

Similarly, minimizing the number of seeds (while maintaining dose homogeneity) is important. By doing so, the possibility for “hot spots” is reduced. Moreover, using fewer seeds is economically beneficial. A good treatment plan tries to minimize the number of seeds used.

CHAPTER 3

DATA GENERATION AND MODELING

This chapter aims to describe the methods by which data was generated for the project work. Specifically, a description of DANTSYS, the transport package used, will be given as will be a thorough account of the prostate model and data used. Finally, how these data and models are implemented in MATLAB are discussed.

3.1 DANTSYS: A Neutral Particle Transport Code

A Diffusion Accelerated Neutral-particle Transport SYStem (DANTSYS) [6] was used to generate all the fluxes and currents used throughout this work. Specifically, the module TWODANT for two-dimensional transport was used. DANTSYS is a discrete-ordinates code that solves the Boltzmann transport equation (see pg. 3). A good treatment of discrete-ordinates may be found in Lewis and Miller [9], but it helps to describe the method briefly. The discrete-ordinates approach discretizes the angular coordinate Ω into some number of directions. Additionally, the spatial variable \vec{r} is discretized into finite elements. The code solves the angular flux in a given spatial element for each direction via iteration. The scalar flux and current vectors can be found in each spatial element using a weighted sum of the angular fluxes, or

$$\phi(i, E) = \sum_{k=1}^n w_k \psi_{ik}(E) \quad (3.1)$$

and

$$J_x(i, E) = \sum_{k=1}^n \mu_k w_k \psi_{ik}(E), \quad (3.2)$$

respectively. Here, i denotes the i th voxel, w_k is the weight for a direction k , μ_k is the cosine of the angle between k and \hat{x} (with similar definitions for J_y and J_z), and n is the total number of directions.

Multigroup Libraries

Furthermore DANTSYS treats particle transport via a multigroup approach. The continuous energy spectrum of particles is also discretized into finite energy groups; thus our flux becomes $\phi(i, g)$ for a voxel i and energy group g . The cross-section data for these groups are compiled in several libraries. In this work, we use a broad three photon group library generated from the lowest three energy groups of the FENDL-42 group photon library. The average photon energy of ^{125}I , the isotope used in seeds in this work, falls in the first energy group spanning 20-30 keV. The second and third groups span 10-20 keV and 1-10 keV, respectively [8].

Fluxes and Currents

DANTSYS has the scalar flux as an available output, so no secondary routine is needed to compute the scalar flux from angular flux information. One need only a routine to read the code's binary Fortran file to manipulate the flux information as needed. Such a routine is provided as Appendix A. On the other hand, the current is not available as output; thus, a routine for computing the current was needed. Marat Seydaliev graciously provided routines from which the one given in Appendix B was adapted.

3.2 Prostate Model: Adjoint Fluxes and Current Generation

The prostate model used is based on a set of three-dimensional ROI's used by Chaswal [2]. The model spans $60\text{ mm} \times 55\text{ mm}$ in the plane contained in ultrasound images. Additionally, there are 14 such planes, i.e. 14 ultrasound images, each separated by 5 mm. Because this work presents algorithms treated in only two-dimensions, we have taken a subset of these images and their associated ROI's as the foundation to the models used herein.

A DANTSYS input was prepared for each ROI of five ultrasound slices (numbers 3, 5, 7, 9, and 11 of the original 14); thus, with four tissues, there are twenty such inputs. As an example, the input for the tumor region of slice 7 is provided in Appendix C. The treatment plane is defined by voxels of 1 square mm to coincide with the ultrasound resolution. The total width and height of the planes are 60 mm and 55 mm, respectively. Each pixel coinciding with the ROI is set to 1; those outside the ROI are set to 0. The entire treatment plane consists of water.

Because these inputs are generating adjoint fluxes, the ROI defines the adjoint source, i.e. the detector of interest. For consistency, we present these fluxes instead as the adjoint function (thus with units of Gy/S_u , where 1 S_u corresponds to a single 0.43 mCi seed). The adjoint functions and adjoint ratio for slice 7 are given in Fig. 3.1. In the generation of the adjoint fluxes, it was possible to employ a *ray tracing first collision source*. This feature essentially transports particles from their initial point of generation to the point of their first collision without subjecting their paths to the effects of spatial-angular discretization. The distribution of all these new, “first collision” points becomes a new, “first collision” source spectrum. By doing this, so-called *ray effects* due to the discrete-ordinates method are avoided. With ray tracing, an S_N order of 8 was found to be adequate for the adjoint flux calculations.

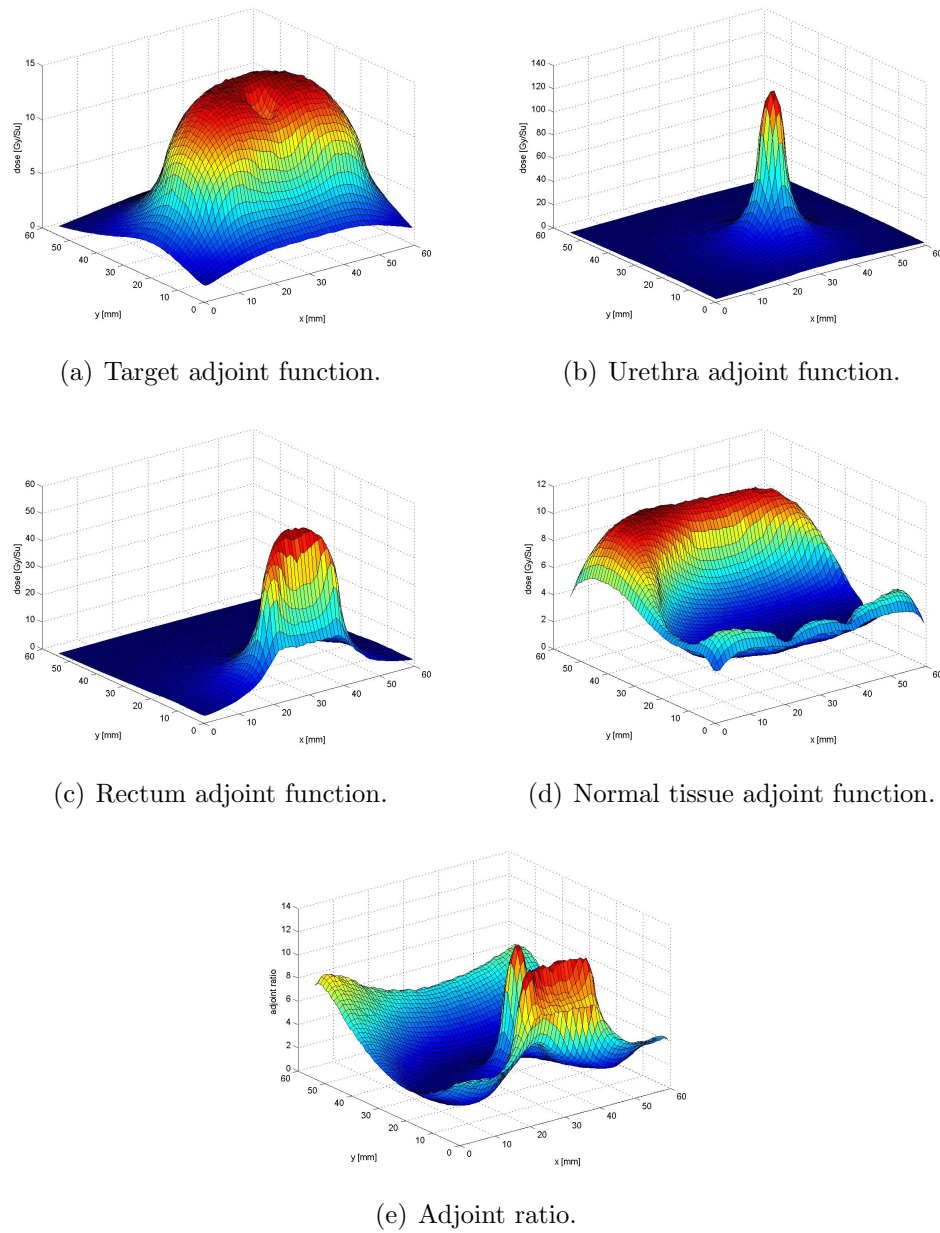


Figure 3.1: Adjoint functions and ratio for slice 7.

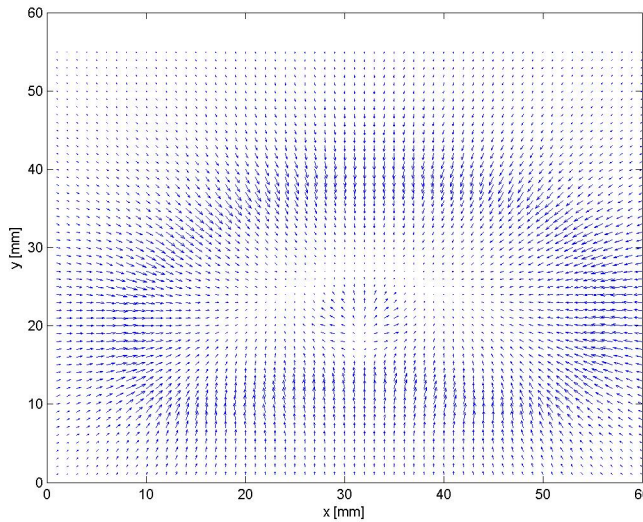


Figure 3.2: Target Current, Slice 7.

To generate the adjoint current, slightly modified inputs were necessary because the angular flux files are unavailable when a first collision source is used. Therefore, these new files did not employ ray tracing. To help mitigate possible ray effects, an S_N order of 16 was used. For the target and normal tissues, ray effects were largely avoided; however, for the smaller urethra and rectum, some rippling effects in the current can be seen.

Figs. 3.2-3.5 show the direction fields for the currents of slice 7. Fig. 3.6 shows contour plots of the normed current, $J_N = \|\mathbf{J}(i)\| = \sqrt{J_x^2(i) + J_y^2(i)}$, for both the target and urethra. Note that ray effects in the urethra current are present.

3.3 Seed Model: Forward Current and Dose Profiles

The previous work on Greedy methods focused primarily on the use of model 6711 ^{125}I seeds. While certainly possible to model in three-dimensions, it was hard to determine how best to model this source in two-dimensions. In the end, it was believed using

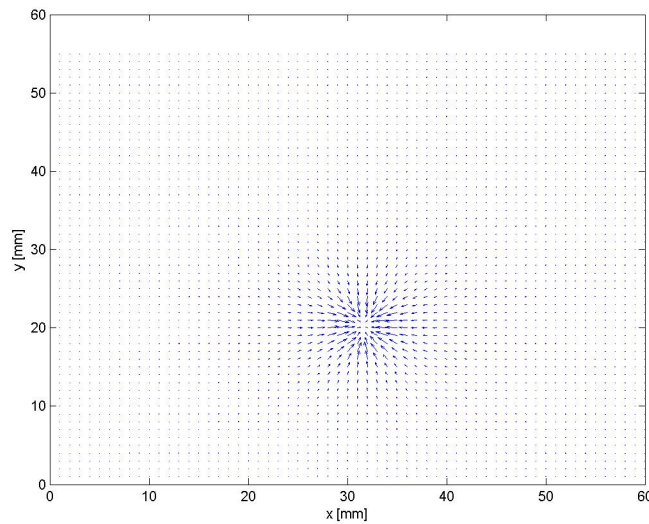


Figure 3.3: Urethra Current, Slice 7.

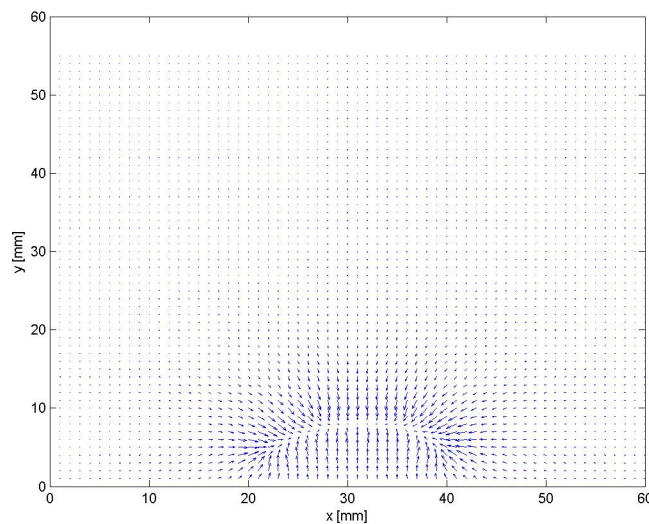


Figure 3.4: Rectum Current, Slice 7.

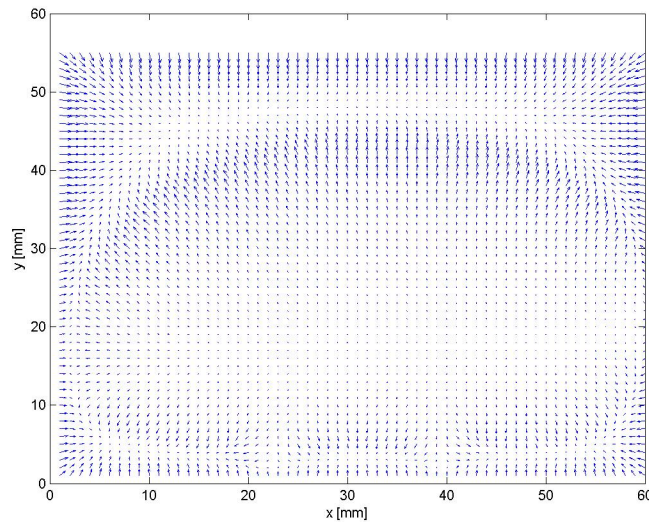
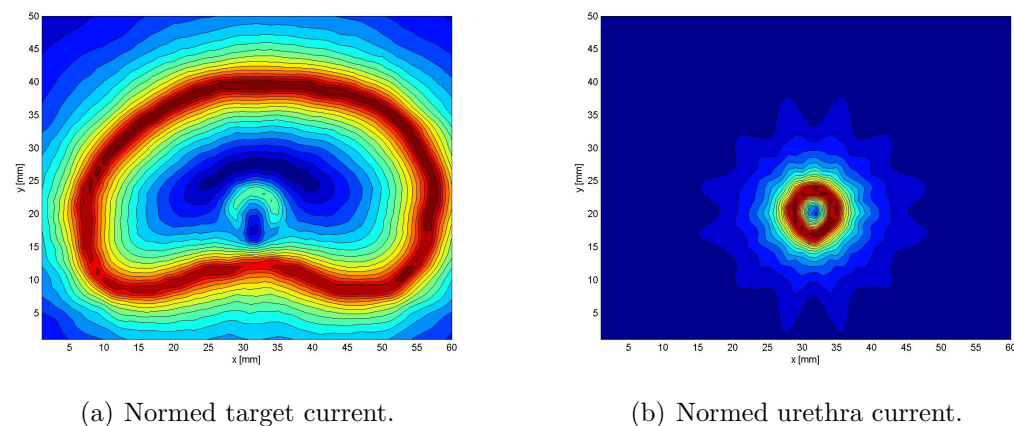


Figure 3.5: Normal Current, Slice 7.



(a) Normed target current.

(b) Normed urethra current.

Figure 3.6: Normed current for target and urethra, slice 7.

Energy (MeV)	DF $\frac{(rem/hr)}{(p/cm^2-s)}$
0.005	1.229e-5
0.010	2.780e-6
0.015	1.952e-6
0.020	5.880e-7
0.025	3.719e-7
0.030	2.560e-7

Table 3.1: ICRP-21 Flux-to-dose Conversion Factors.

a small cluster of 1 mm voxels as the forward source definition and then normalizing it to 0.43 mCi would suffice. The source model used throughout is a 1 mm voxel with an additional 1 mm voxel adjacent to each side; thus, five voxels define the seed. Material effects, i.e. the titanium sheath and other components making up the seed, are not included; the seed consists simply of a photon source centered in a water medium.

To compute the dose, the ICRP 21 flux-to-dose conversion factors (DF) were used [7]. Table 3.1 provides these constants for the energies of interest. Log-log interpolation was used to find the DF values not listed in the report; these are included with the actual tabulated values, denoted via bold font. The DF values at mid-group were used to calculate energy-weighted dose, defined by $dose(i) = \sum_g \phi_g(i)$. Fig. 3.7 provides a mesh plot of the seed dose profile using these constants.

Previous work has employed the AAPM Task Group 43 recommendations for ^{125}I dosimetry [11]. A comparison between the midaxial plane of this distribution for a 1 S_u seed and the two-dimensional 1 S_u seed from above was performed. The TG-43 definition has significantly higher dropoff than does the two-dimensional model. This is expected, because the three-dimensional seed incorporates axial falloff in addition to radial falloff; the two-dimensional model has only radial falloff. A plot comparing

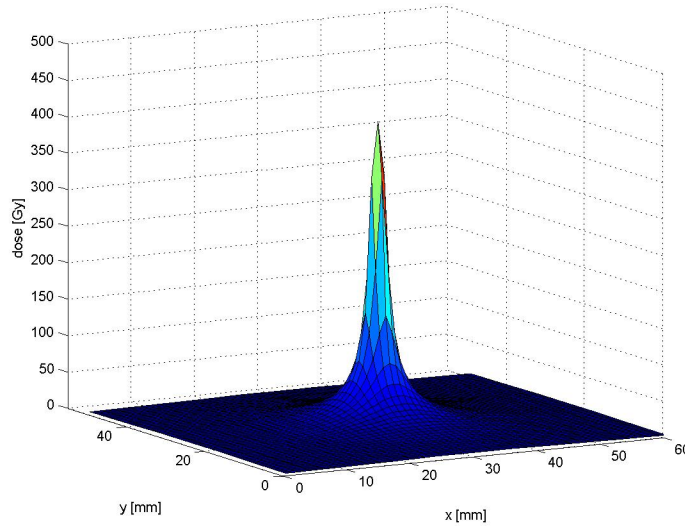


Figure 3.7: Dose Profile for 2-D Seed Model.

the midaxial TG-43 and the two-dimensional radial profiles is given in Fig. 3.8.

One might wonder why the TG-43 dose profile was not used. In short, it easily could have been used, but two reasons suggest using the two-dimensional case (with a multiplicative factor). First, there is no way to compute the current associated with the TG-43 protocol; since the current is foundational for this work, it was thought best simply to derive all the data used from one set of models. Second, the dose profile for TG-43 falls off rapidly as noted. Because we are confined to a planar solution space, more seeds are most likely needed to cover the volume represented than would be true for a three-dimensional problem. Hence, excessive over-dosing would arise due to many areas with dose greater than 800 Gy. To avoid this, the modeled seed profile is used.

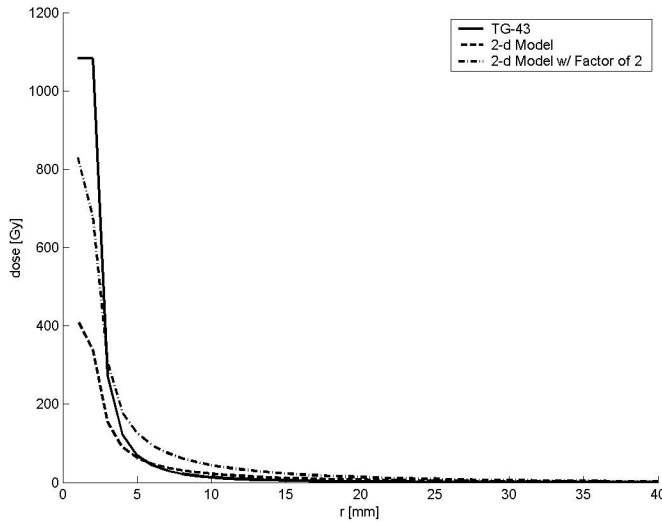


Figure 3.8: Comparison of 2-D Model and TG-43 Radial Dose Profile.

3.4 Implementation in MATLAB

The MATLAB environment is used for all the treatment planning presented in this work. All ROI's are contained in binary mask files that represent the contours originally drawn on ultrasound images. See Fig. 3.9 for a representative tumor contour and Fig. 3.10, its binary mask representation.

This work retains many of the same basic MATLAB constructs as Chaswal and others. However, working in only two-dimensions has changed indexing and matrix sizes. The most important matrix quantities, their dimensions and their notation as used in the code are provided in Table 3.2. The quantity *tissue* represents one of the ROI names, and for *tisGeo*, *tis* is one of *t*, *u*, *r*, or *n*.

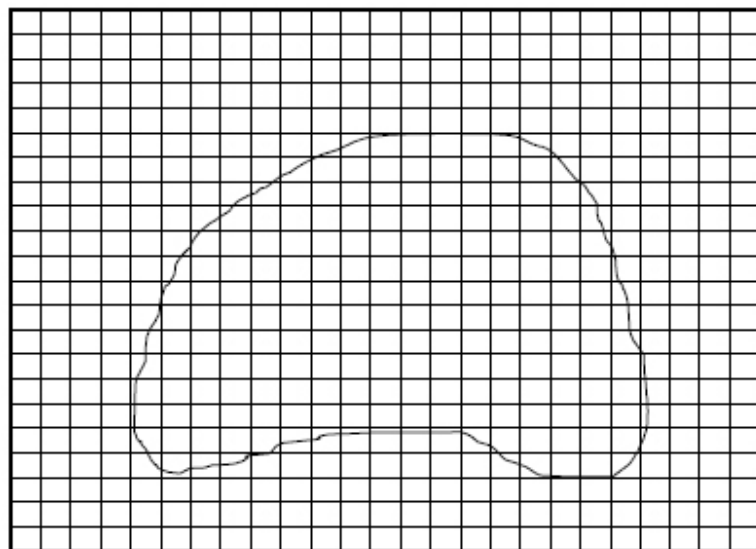


Figure 3.9: Schematic target outline [2].

Figure 3.10: Binary mask file for target [2].

Information	Notation	Size
Seed Dose Profile	$sDdose(i, j)$	[150,160]
Seed Current	$sDcur(i, j)$	[150,160]
Adjoint function	$tissue(i, j)$	[60,55]
Patient ROI	$tisGeo(i, j)$	[60,55]
Dose Distribution	$dose2d(i, j)$	[60,55]
Seed Configuration	$X(i, j)$	[60,55]

Table 3.2: Matrix Dimensions and Their Notation.

CHAPTER 4

CURRENT-DISPLACEMENT: A “NUDGE”

4.1 Theory

The previous section discusses the most recent formulation of an adjoint flux-based greedy heuristic. In this section, a method is presented that takes the seed placement generated by that greedy heuristic and applies a displacement based on the forward and adjoint current defined previously.

In a sense, the greedy heuristic gives to us an initial value from which we can converge toward a better solution using the more detailed information intrinsic to currents. That is to say, given the adjoint (and forward) current contains angular information and not just a scalar quantity, it necessarily provides a more complete description and therefore may generate better insight to the physical nature of the problem. Consequently, it was thought such information could—if used properly—yield better results.

4.2 Defining Current-displacement

Both the forward and adjoint currents as generated via DANTSYS are defined as a two-component vector comprised of a horizontal and vertical current, $\hat{x}J_x$ and

$\hat{y}J_y^1$. Using these data, we may sum the tissue horizontal currents to produce a total weighted horizontal current via

$$J_x^{tot}(i) = w_r J_x^r(i) + w_u J_x^u(i) + w_n J_x^n(i) + w_t J_x^t(i) \quad (4.1)$$

and doing likewise for the vertical component, we have

$$J_y^{tot}(i) = w_r J_y^r(i) + w_u J_y^u(i) + w_n J_y^n(i) + w_t J_y^t(i) \quad (4.2)$$

where each weight coefficient w_i is set to $1/V_i$ for the sensitive tissue, i.e. the urethra, rectum, and normal tissues, and $-1/V_i$ for the target. V_i is the volume of the given tissue. The target term is negated due to our interest in particles traveling *to* it rather than away, as is the case for the other tissues. We can write the current more succinctly using the notation

$$\vec{J}^{tot}(i) = \hat{x}J_x^{tot}(i) + \hat{y}J_y^{tot}(i). \quad (4.3)$$

From the Greedy method, we are given an initial seed placement. We may then superimpose onto our total current at each seed location the forward current calculated via the simple seed model.

This gives us everything we need to calculate the *current-displacement* (\vec{C}) vector. The essential idea is that the currents in the x- and y-directions from the sensitive tissue may act as a *pushing* mechanism used to shift the seeds from their initial placement. However, to avoid seed clustering, we include the forward current from a seed to act on all other seeds. In this way, we define quantitatively the

¹It is helpful to recall that many variables described, e.g. \vec{J} , \vec{C} , etc, are two-dimensional *matrices*; that is to say, $\vec{J}(i)$ denotes the value of \vec{J} at the i th voxel.

current-displacement for a seed at i

$$\vec{C}'(i) = a \left(-\vec{J}^{tot}(i) + b \sum_{\substack{j=1 \\ j \neq i}}^n \vec{J}^s(i, j) \right) \quad (4.4)$$

where $\vec{J}^s(i, j)$ denotes the two-component current at i from a seed at j , b is a constant defining the relative importance of the seed currents to the tissue currents, and a is a constant that converts the summed current magnitudes into a suitable seed displacement value. (The negative before $\vec{J}^{tot}(i)$ is included to show explicitly that the tissue currents must be negated to provide a *push*. This is because the adjoint current represents the flow of particles *to* the adjoint source, namely the tissue of interest; here, we want a flow *away* from that source.)

Initially, trial-and-error was used to investigate values for a and b . However, it quickly became apparent that a more automated approach was needed to account for the various magnitudes of the tissue and seed currents in each problem. Using the manual values as a guide, a suitable definition to relate the seed and tissue currents was found to be

$$b = \max |\vec{J}^{tot}|_2 / (k \max |\vec{J}^s|_2), \quad (4.5)$$

where max refers to the highest value of the given function throughout the treatment plane and

$$k = 1 / \sqrt{m_1 \sqrt{m_2 / m_1}}. \quad (4.6)$$

Here, m_1 and m_2 are the averages of the squared seed and tissue currents, respectively, or

$$m_1 = \text{mean}((J_x^s)^2 + (J_y^s)^2) \quad (4.7)$$

and

$$m_2 = \text{mean}((J_x^{tot})^2 + (J_y^{tot})^2). \quad (4.8)$$

Thus, the relation bears resemblance to the statistical quantity root-mean-square.

Finally, the constant defining the subsequent displacement, a , is defined

$$a = k / \max |\vec{J}^{tot}|. \quad (4.9)$$

These relationships are rather complicated, but they do afford an automated approach to current-displacement, and as will be seen, work fairly consistently for the five problems tested.

Given that the model investigated has a solution space of resolution 1 mm (or with a grid, 5 mm), the displacement must be an integer. It is assumed simply rounding the displacement will suffice. Hence, the applied displacement for a seed at i is defined

$$\vec{C}(i) = \text{round}(\vec{C}'(i)). \quad (4.10)$$

Important to note is how the current-displacement is applied; we do so via

$$i' = (x, y)' \longleftarrow (x + \vec{C}_x(i), y + \vec{C}_y(i)) = i + \vec{C}(i) \quad (4.11)$$

where a seed at position i (with coordinates x and y) is displaced to a position i' .

Because \vec{C} is defined such that all seeds can simultaneously be displaced, the question arises whether displacing all, some, or just one of the seeds at a time is optimal. Using the constants a and b as defined above, allowing for displacement of all seeds typically does not yield a displacement of all seeds, as the minimum displacement is limited by the rounding of Eq. 4.10. To allow for the selective

displacement, we need a ranking criterion; here, the L₂ norm of \vec{C} suffices and is defined

$$\|C(i)\|_2 = \sqrt{C_x(i)^2 + C_y^2(i)} \quad (4.12)$$

Thus, some number of seeds with the highest normed \vec{C} can be selected for displacement.

Additionally, more than one displacement may be desirable. In particular, it may happen after one displacement that a given seed is subjected to a greater \vec{C} value than previously and should therefore be moved. On the other hand, allowing the process to go *ad infinitum* is even less appealing. To account for this, we must include a factor that diminishes \vec{C} with each iteration. We redefine Eq. 4.10

$$\vec{C}(i) = \text{round}(\vec{C}'(i)/it^c). \quad (4.13)$$

where c is a constant defining by how much \vec{C} should diminish at iteration it ; $c = 1$ for this study. Note that Eq. 4.11 still defines the displacement applied, but now for the dynamic \vec{C} of 4.13. The number of iterations can be limited by a given maximum, or equally viable, the iterations could cease when successive values for $\|\vec{C}\|_2$ differ by less than some threshold value.

Putting this altogether, Alg. 2 defines the greedy heuristic with current-displacement.

4.3 Results and Discussion

In this section, a comparison is made between the greedy heuristic (GY) using and without using the current-displacement (CD). For this study, no treatment grid was used for either GY or CD. For CD, all seeds were allowed to be displaced. Three cases are presented, one corresponding for each of seed strength $f = 1$, $f = 2$, and $f = 3$.

```

Input: Seed locations from greedy heuristic
Output: New seed locations
it  $\leftarrow 0$ ;
while  $it \leq itmax$  do
    it  $\leftarrow it + 1$ ;
     $\vec{C}_x \leftarrow -\vec{J}_x^{tot}$ ;
     $\vec{C}_y \leftarrow -\vec{J}_y^{tot}$ ;
    foreach seed  $s(i)$  ( $i$  being its location) do
        to  $\vec{C}_x$ , add  $b \times \vec{J}_x^s$  centered at  $i$  ;
        to  $\vec{C}_y$ , add  $b \times \vec{J}_y^s$  centered at  $i$  ;
         $||\vec{C}|| \leftarrow \sqrt{C_x^2 + C_y^2}$ ;
    end
    sort seeds in order of decreasing  $||\vec{C}||$  ;
    foreach of the first number of seeds  $s(i)$  to be displaced do
         $\vec{C}(i) \leftarrow \text{round}(\vec{C}(i)/it)$ ;
         $i \leftarrow (x, y) \leftarrow (x + a\vec{C}_x(i), y + a\vec{C}_y(i)) \leftarrow i + a\vec{C}(i)$ ;
    end
end

```

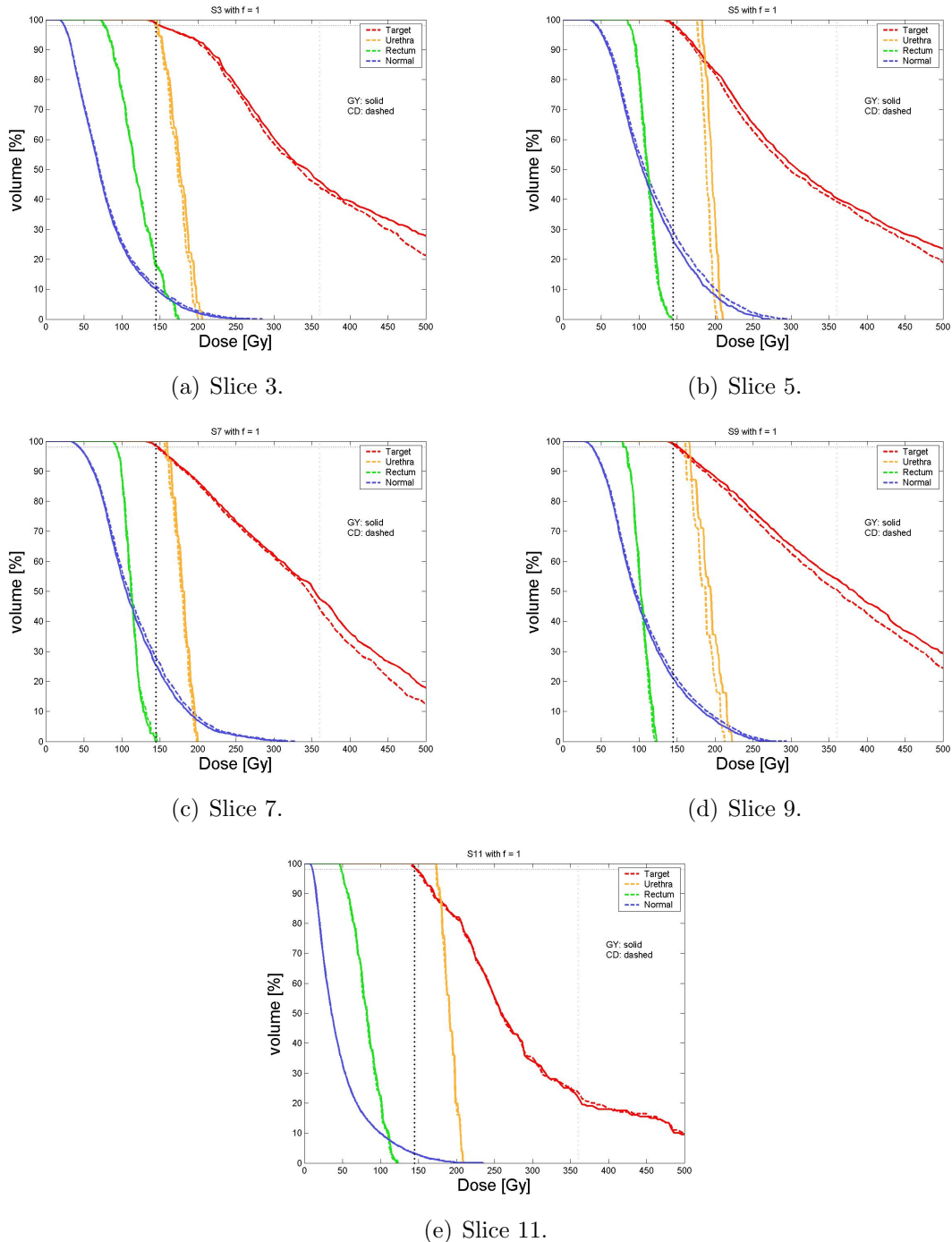
Algorithm 2: Greedy heuristic with current-displacement.

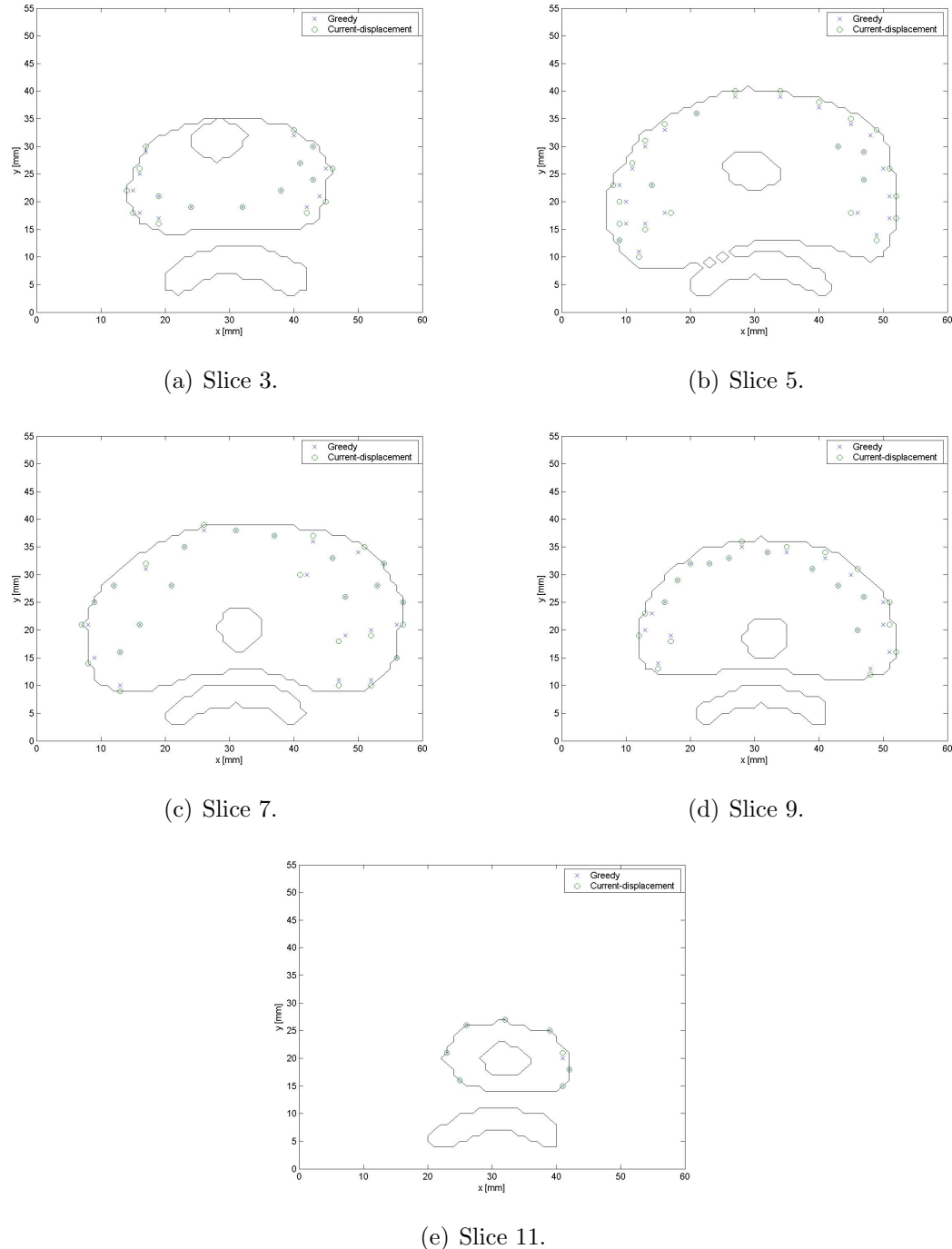
By looking at higher strengths, the number of seeds used is closer to what is found on a given plane for a three-dimensional problem. This is due mainly to the highly restricted planar solution space; in other words, using the same strength seed ($f = 1$) used in a three-dimensional case necessarily requires a greater number of seeds *on the plane* to cover a given area than in three-dimensions, where the seeds on the plane of interest have in their proximity other seeds on other planes.

For each case a table is first provided of the aforementioned evaluation parameters. Thereafter, dose-volume histograms (DVH) and the seed placement for each problem are given. Note for the tables that **S3** represents “slice 3” of the original three-dimensional problem and similarly for the other labels provided. Furthermore, note for the DVH’s that two vertical lines correspond to 145 Gy and 360 Gy and that a horizontal line corresponds to 98 volume %.

		S3	S5	S7	S9	S11
TARGET						
$V_{100}(\%)$	<i>CD</i>	98.16	97.49	98.06	98.69	98.00
	<i>GY</i>	98.35	98.27	98.06	98.92	98.50
$V_{150}(\%)$	<i>CD</i>	87.68	73.85	81.13	82.08	73.00
	<i>GY</i>	88.42	75.76	81.29	83.51	72.00
CN	<i>CD</i>	0.49	0.56	0.58	0.51	0.42
	<i>GY</i>	0.50	0.59	0.60	0.53	0.43
DNR	<i>CD</i>	0.89	0.76	0.83	0.83	0.74
	<i>GY</i>	0.90	0.77	0.83	0.84	0.73
URETHRA						
$V_{125,ur}(\%)$	<i>CD</i>	30.56	83.78	40.63	54.84	76.00
	<i>GY</i>	41.67	100.00	50.00	70.97	76.00
$V_{360,ur}(\%)$	<i>CD</i>	0.00	0.00	0.00	0.00	0.00
	<i>GY</i>	0.00	0.00	0.00	0.00	0.00
$D_{90,ur}(\text{Gy})$	<i>CD</i>	153.01	180.53	163.04	162.90	177.29
	<i>GY</i>	154.40	186.18	166.15	169.37	178.66
RECTUM						
$V_{80,re}(\%)$	<i>CD</i>	50.34	32.23	38.39	9.90	1.80
	<i>GY</i>	49.66	38.02	37.50	12.87	2.70
$V_{90,re}(\%)$	<i>CD</i>	87.25	96.69	99.11	86.14	35.14
	<i>GY</i>	85.91	96.69	99.11	86.14	36.04
$D_{90,re}(\text{Gy})$	<i>CD</i>	88.97	95.95	99.97	89.36	57.75
	<i>GY</i>	88.80	96.48	99.60	89.30	58.19
NORMAL TISSUE						
$V_{90,no}(\%)$	<i>CD</i>	35.47	62.26	65.35	54.21	16.41
	<i>GY</i>	34.19	61.15	62.88	53.94	16.38
QUALITATIVE						
<i>Seeds</i>	<i>GY</i>	16	25	27	22	8
	<i>CD</i>	16	25	27	22	8

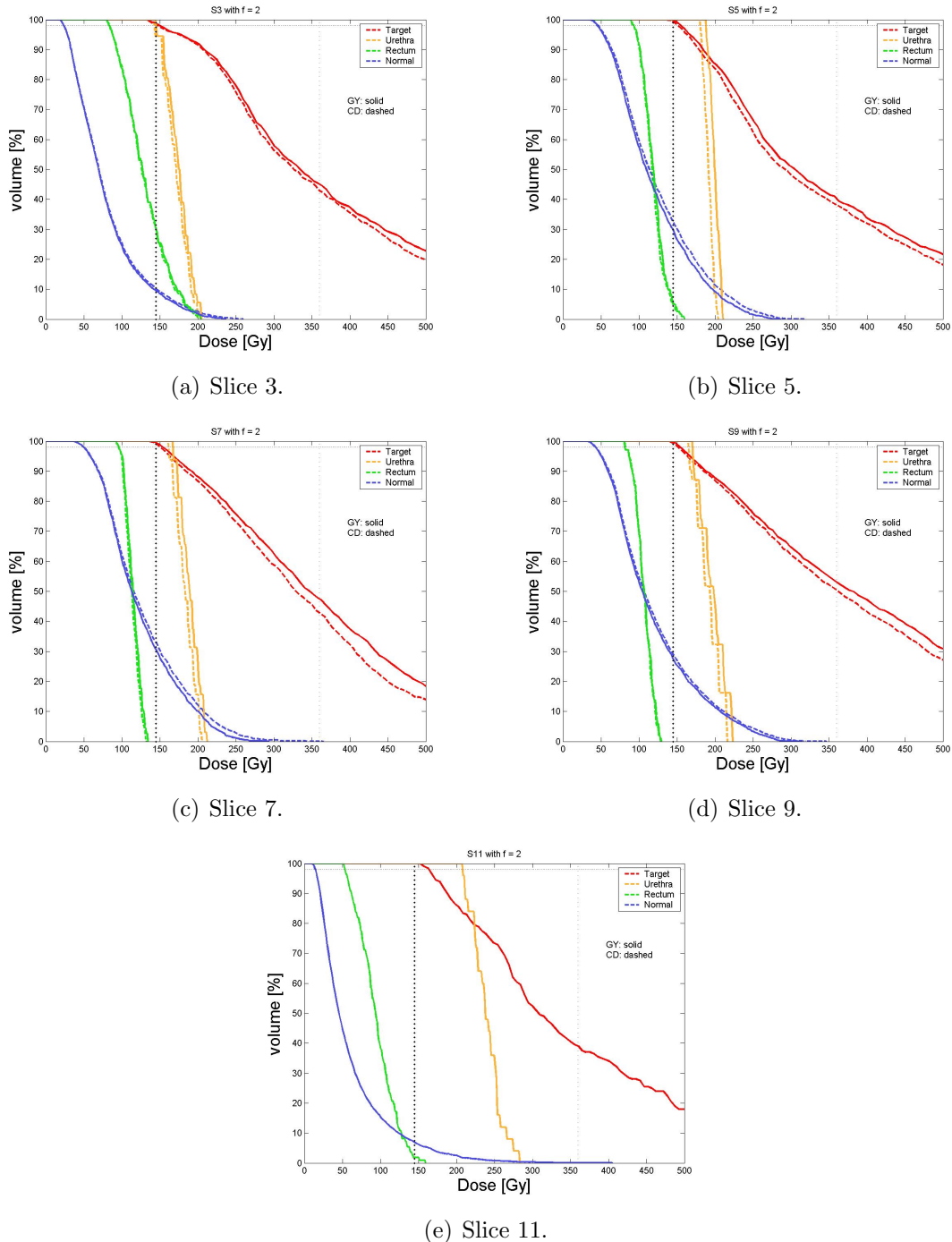
Table 4.1: Evaluation parameters for $f = 1$

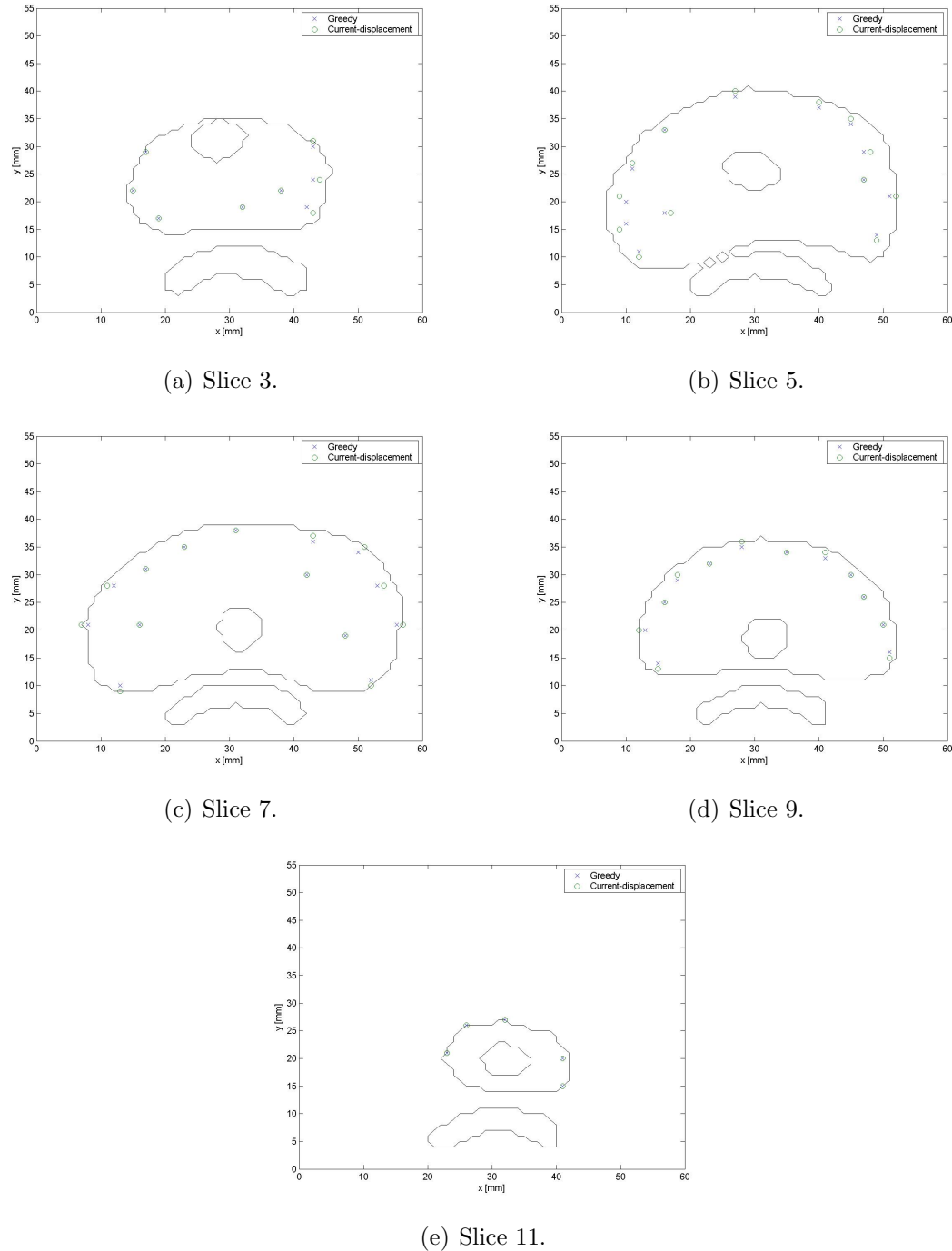
Figure 4.1: DVH's for each slice with $f = 1$.

Figure 4.2: Seed placements, $f = 1$.

		S3	S5	S7	S9	S11
TARGET						
$V_{100}(\%)$	<i>CD</i>	98.16	98.70	98.55	98.92	100.00
	<i>GY</i>	98.35	99.31	99.19	99.28	100.00
$V_{150}(\%)$	<i>CD</i>	86.40	76.28	81.37	82.44	81.00
	<i>GY</i>	87.87	78.79	83.79	82.92	81.00
CN	<i>CD</i>	0.50	0.55	0.56	0.48	0.35
	<i>GY</i>	0.51	0.58	0.58	0.48	0.35
DNR	<i>CD</i>	0.88	0.77	0.83	0.83	0.81
	<i>GY</i>	0.89	0.79	0.84	0.84	0.81
URETHRA						
$V_{125,ur}(\%)$	<i>CD</i>	27.78	94.59	53.13	70.97	100.00
	<i>GY</i>	36.11	100.00	68.75	74.19	100.00
$V_{360,ur}(\%)$	<i>CD</i>	0.00	0.00	0.00	0.00	0.00
	<i>GY</i>	0.00	0.00	0.00	0.00	0.00
$D_{90,ur}(\text{Gy})$	<i>CD</i>	153.00	182.81	167.72	169.90	211.59
	<i>GY</i>	155.56	190.80	173.17	173.36	211.59
RECTUM						
$V_{80,re}(\%)$	<i>CD</i>	62.42	52.07	37.50	20.79	20.72
	<i>GY</i>	63.09	57.02	44.64	21.78	20.72
$V_{90,re}(\%)$	<i>CD</i>	92.62	100.00	100.00	91.09	54.95
	<i>GY</i>	93.29	98.35	100.00	91.09	54.95
$D_{90,re}(\text{Gy})$	<i>CD</i>	93.67	101.17	101.48	91.46	62.56
	<i>GY</i>	93.22	101.70	102.84	91.71	62.56
NORMAL TISSUE						
$V_{90,no}(\%)$	<i>CD</i>	33.66	64.96	70.91	62.20	22.21
	<i>GY</i>	34.20	62.77	70.19	60.20	22.21
QUALITATIVE						
<i>Seeds</i>	<i>GY</i>	8	13	14	12	5
	<i>CD</i>	8	13	14	12	5

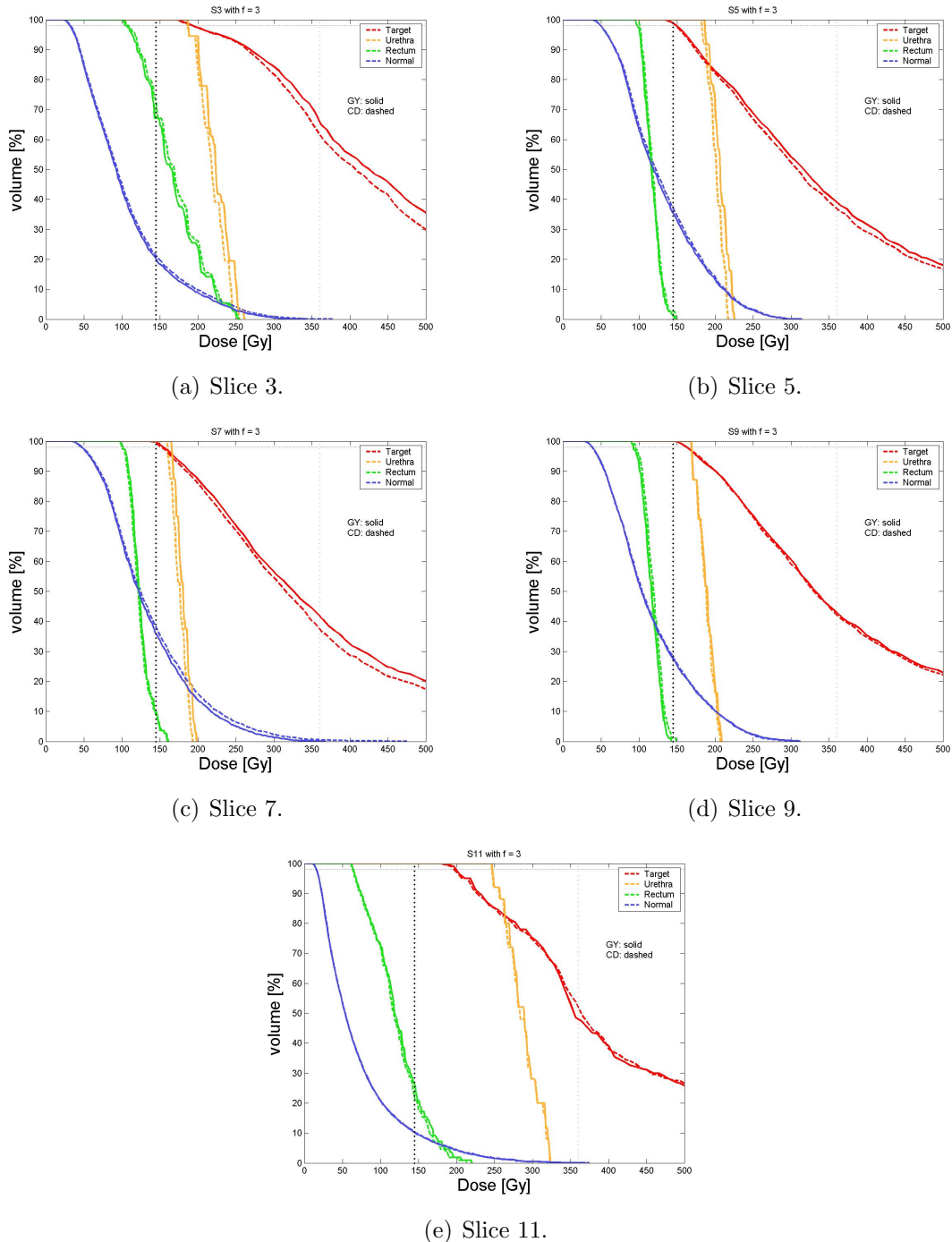
Table 4.2: Evaluation parameters for $f = 2$

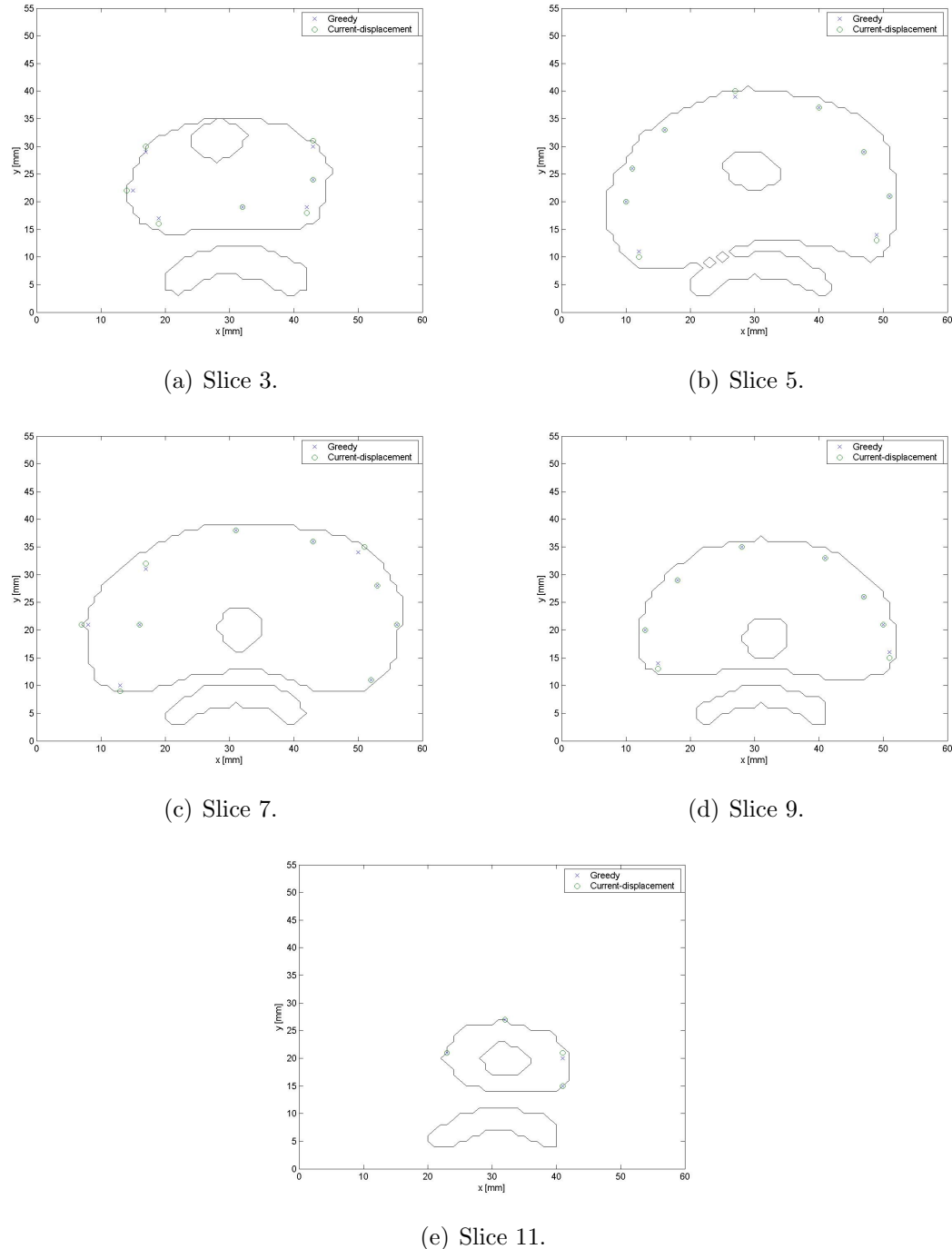
Figure 4.3: DVH's for each slice with $f = 2$.

Figure 4.4: Seed placements, $f = 2$.

		S3	S5	S7	S9	S11
TARGET						
$V_{100}(\%)$	<i>CD</i>	100.00	98.01	98.95	100.00	100.00
	<i>GY</i>	100.00	98.18	99.19	100.00	100.00
$V_{150}(\%)$	<i>CD</i>	95.59	76.02	80.08	83.39	91.50
	<i>GY</i>	95.40	77.23	81.77	85.07	95.00
CN	<i>CD</i>	0.39	0.53	0.55	0.47	0.29
	<i>GY</i>	0.39	0.54	0.56	0.48	0.28
DNR	<i>CD</i>	0.96	0.78	0.81	0.83	0.92
	<i>GY</i>	0.95	0.79	0.82	0.85	0.95
URETHRA						
$V_{125,ur}(\%)$	<i>CD</i>	100.00	100.00	34.38	67.74	100.00
	<i>GY</i>	100.00	100.00	40.63	70.97	100.00
$V_{360,ur}(\%)$	<i>CD</i>	0.00	0.00	0.00	0.00	0.00
	<i>GY</i>	0.00	0.00	0.00	0.00	0.00
$D_{90,ur}(\text{Gy})$	<i>CD</i>	198.72	189.27	163.34	170.91	257.05
	<i>GY</i>	201.32	192.93	167.79	171.63	257.98
RECTUM						
$V_{80,re}(\%)$	<i>CD</i>	95.97	55.37	66.07	56.44	50.45
	<i>GY</i>	92.62	48.76	71.43	51.49	55.86
$V_{90,re}(\%)$	<i>CD</i>	100.00	100.00	100.00	100.00	78.38
	<i>GY</i>	100.00	100.00	100.00	99.01	79.28
$D_{90,re}(\text{Gy})$	<i>CD</i>	123.94	104.35	107.66	104.61	74.34
	<i>GY</i>	120.61	103.95	108.94	102.01	75.56
NORMAL TISSUE						
$V_{90,no}(\%)$	<i>CD</i>	45.12	70.57	71.25	55.65	24.25
	<i>GY</i>	44.01	70.49	69.68	55.96	23.96
QUALITATIVE						
<i>Seeds</i>	<i>CD</i>	7	9	10	8	4
	<i>GY</i>	7	9	10	8	4

Table 4.3: Evaluation parameters for $f = 3$

Figure 4.5: DVH's for each slice with $f = 3$.

Figure 4.6: Seed placements, $f = 3$.

Target Irradiation

From Tables 4.1-4.3, we note that only S5 for $f = 1$ has V_{100} which has moved below the required 98% target coverage. Furthermore, recall that V_{150} measures high dose regions within the target. In every case but two, for S11 with $f = 1$ and S3 with $f = 3$, applying the current-displacement reduces this percentage. In all but those cases, the DNR is also seen to decrease (i.e. improve) upon displacement. The average DNR values over all cases for GY and CD are 0.8311 and 0.8477 (appx. 2.0% change), respectively.

Contrarily, CN drops for all but the latter of those cases, which begs the question whether these two criteria can be simultaneously improved. The average CN values over all cases for GY and CD are 0.4919 and 0.4839 (appx. 1.6% change), respectively. Overall, applying current-displacement slightly improves the quality of the dose received by the target.

Urethra Sparing

Tables 4.1-4.3 indicate that $V_{360,ur}$ is zero for all cases considered. Note furthermore that both $D_{90,ur}$, the minimum dose to 90% of the urethra, and $V_{125,ur}$, the urethral volume receiving $1.25D_p$, are decreased via application of CD in all cases where seeds are dispersed. The average $D_{90,ur}$ values over all cases for GY and CD are 183.40 Gy and 180.07 Gy, respectively. This means, on average, that CD reduces $D_{90,ur}$ by 1.6%. Additionally, the average $V_{125,ur}$ values over all cases for GY and CD are 75.29% and 68.96%, showing CD decreases this urethral “hot spot” metric by about 8.4%.

Figs. 4.1, 4.3, and 4.5 show explicitly the reduced urethral dose. Overall, applying current-displacement improves sparing of the urethra.

Rectum

As mentioned above, $D_{90,re}$ is a good threshold measure for rectal bleeding. From Tables 4.1-4.3, the CD offers no improvement, with about an equal number of cases being slightly higher and slightly lower than for GY. The same is true for $V_{90,re}$ ². For $V_{80,re}$, the rectal volume receiving $0.8D_p$, the results are more spread out. However, on average GY and CD achieve $V_{80,re}$ values of 44.54% and 43.19%, meaning CD reduces rectal “hot spots” by about 3%. Thus, applying current-displacement improves rectal sparing.

Normal Tissue Sparing

The average $D_{90,no}$ values over all cases for GY and CD are 49.48 Gy and 50.30 Gy, respectively, which means the CD results in a slightly higher dose to normal tissue (appx. 1.6% increase). Figs. 4.1, 4.3, and 4.5 depict this slight increase for most of the individual cases. Overall, normal tissue sparing is slightly reduced.

General Remarks

From the evaluation data, it is clear CD does give rise to sensitive tissue sparing. While the normal tissue dose does increase with CD, the magnitude of that increase is slightly smaller than the improvements seen for the urethra and rectum. Furthermore, since the target dose coverage of 98% is met except for one case, it is possible to say, on average, that the treatment plans as generated with CD are better than those

²It should be observed that $V_{90,re}$ all around is too high. While for cases here, a value around 90% is about average, for a proper three-dimensional case, this value is closer to 60%. This phenomenon is found for other parameters. Most likely, such distorted values are due first to the two-dimensional nature of the problem and second to the shape of the dose profile used which is necessarily different than is found in three-dimensions.

without CD.

Additionally, from Figs. 4.2, 4.4, and 4.6, it seems in some cases the seeds have escaped the target region; this is not the case, though for some plans the seeds are on the extreme periphery.

CHAPTER 5

NORMED CURRENT-DISPLACEMENT: A NEW GREEDY CRITERION

While the results from the previous section are promising, it was believed applying current-displacement in another way might yield even better results. The idea is essentially this: *given the current provides more information straightforward than does the flux, then perhaps using the current completely in place of the flux might yield nearer-to-optimal plans.* As will be seen, this can be the case.

5.1 Theory

For the following method, we redefine current-displacement to be

$$\vec{C}'(i) = (\hat{x}J_x^{tot}(i) + \hat{y}J_y^{tot}(i)) . \quad (5.1)$$

Note that seed currents are not included. The summed current from tissues at a voxel i is redefined

$$\vec{J}^{tot}(i) = w_r|\vec{J}^r(i)| + w_u|\vec{J}^u(i)| + w_n|\vec{J}^n(i)| + w_t|\vec{J}^t(i)| . \quad (5.2)$$

where $|\cdot|$ denotes the absolute value. The normed current-displacement remains as defined in Eq. 4.12, or

$$\|\vec{C}(i)\|_2 = \sqrt{C_x(i)^2 + C_y^2(i)}.$$

This function $\|\vec{C}\|_2$ will be our *greedy criterion*, defined in Sec. 2.4.2.

Unlike the last method presented, the current weights w_i are not simply the inverse volumes of tissues. Whereas before the parameters a and b afford a dynamic, automated approach to generating adequate constants for displacing seeds, here, no such displacements occur and therefore no such variables exist. Consequently, we look for an adequate definition of the w_i such that the tissue currents are properly summed to achieve good seed placement, which inverse volumes alone could not provide.

Defining for a tissue i the parameter

$$rms_i = \sqrt{\text{mean}\left((J_x^i)^2 + (J_y^i)^2\right)} \quad (5.3)$$

where rms_i is simply the root-mean-square of the tissue current, we define for each tissue i the weighting factor

$$w_i = 1/rms_i \div \min rms_i, i \in (u, r, n). \quad (5.4)$$

Note that the target is not considered. In studying these parameters manually, in no case did including the target improve the treatment plan; hence, we set $w_t = 0$. In general, the weights are roughly (though dynamic!) 6, 3, and 1, for the urethra, rectum, and normal tissue, respectively.

Using these definitions for the normed current-displacement, a new greedy heuristic is established. In this schematic, the coordinate of least normed current-displacement is chosen for the next seed. However, and as discussed above, a method to disperse seeds is needed, so we employ the aforementioned dose-update scheme (see 2.4.3). Alg. 3 provides a basic schematic for the CD-driven greedy heuristic.

Input: Adjoint currents, seed dose profile, and patient geometry.

Output: Optimized treatment plan.

```

calculate  $w_i$  ;
calculate  $\vec{J}^{tot}$  ;
calculate  $\vec{C}$  ;
sort  $\vec{C}$  in increasing order ;
place first seed at position of least  $\vec{C}$  ;
it  $\leftarrow 0$ ;
 $D_p = 145$  Gy;
dcov  $\leftarrow 98\%$ ;
dose  $\leftarrow$  finddose(seed locations);
 $V_{100} \leftarrow$  findv100(dose);
while  $V_{100} \leq dcov$  or  $it \leq itmax$  do
|  $it \leftarrow it + 1$ ;
|  $\vec{C} \leftarrow \vec{C} \times dose/D_p$ ;
| sort  $\vec{C}$  in increasing order ;
| place next seed at position of least  $\vec{C}$  ;
| dose  $\leftarrow$  finddose(seed locations);
end
```

Algorithm 3: CD-driven greedy heuristic with dose-update.

5.2 Results and Discussion

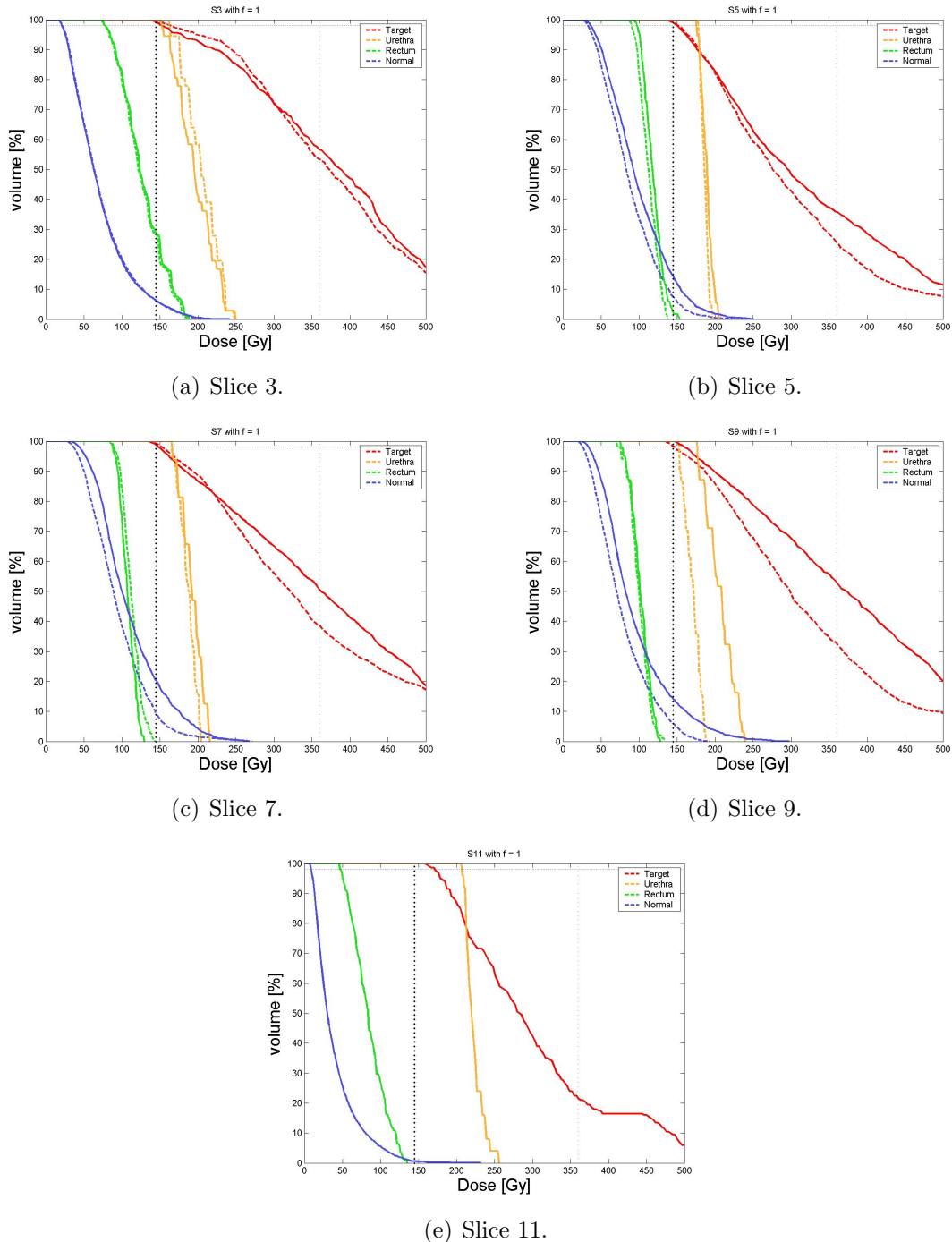
As in the last section, several cases are provided for comparison. For this study, the effect of limiting seed placement to a $5\text{ mm} \times 5\text{ mm}$ treatment grid is examined. For seed strengths of $f = 1$ and $f = 2$, all slices are examined with and without the treatment grid; thus, there are four sets of tables and images. For brevity, we use CD now to refer to the method just described and, as before, GY shall denote the flux-based greedy heuristic.

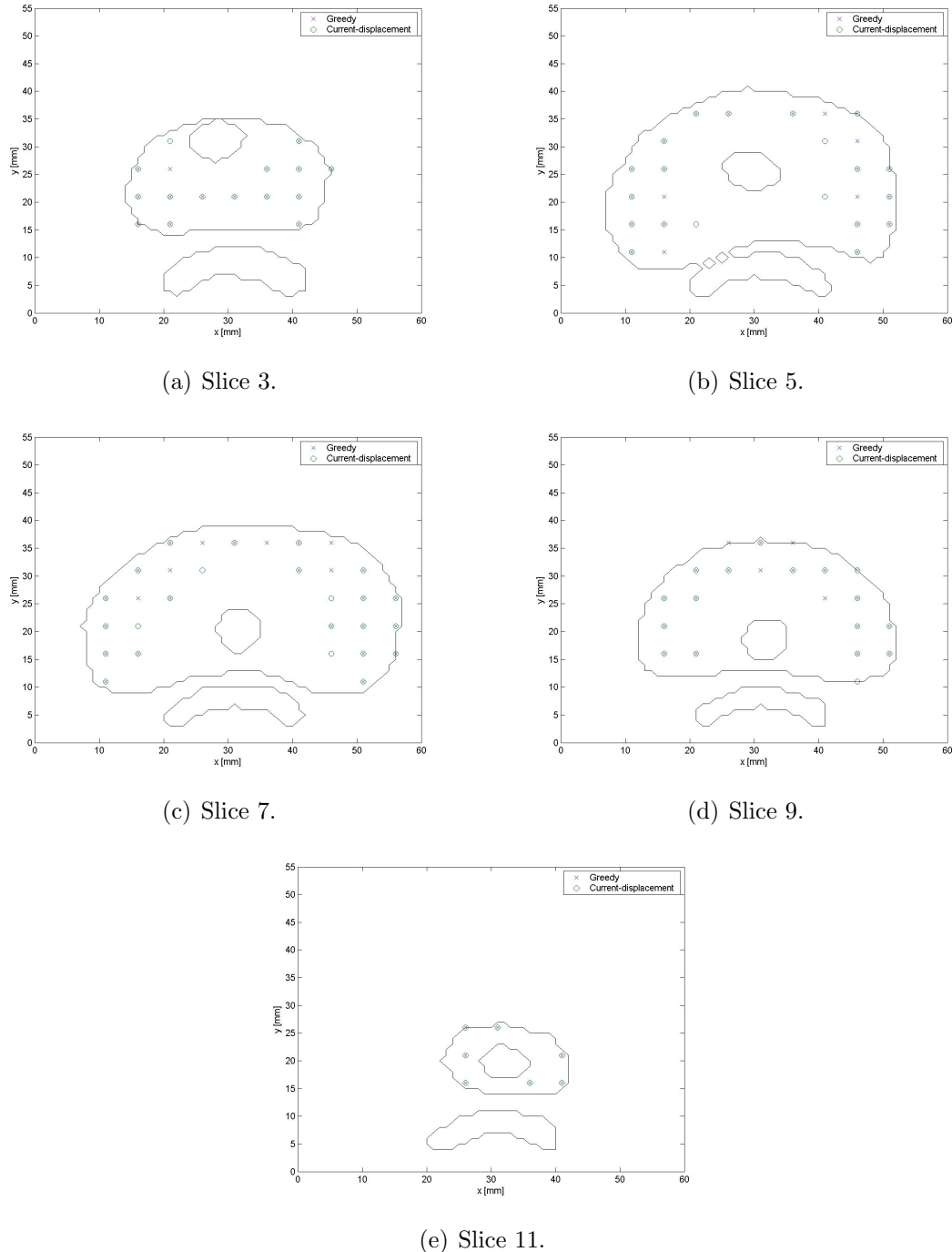
Target Irradiation

We note from Tables 5.1-5.4 that all twenty cases yielded $V_{100} \leq 98\%$. On average, CD yielded a 0.2% gain in V_{100} over GY, a negligible improvement. Additionally, V_{150} for CD is lower than that for GY in 12 cases, and on average, decreases V_{150} by about

		S3	S5	S7	S9	S11
TARGET						
$V_{100}(\%)$	<i>CD</i>	100.00	99.22	99.11	98.09	100.00
	<i>GY</i>	99.08	98.61	98.31	100.00	100.00
$V_{150}(\%)$	<i>CD</i>	93.75	72.21	83.31	79.09	75.00
	<i>GY</i>	90.26	75.06	83.15	86.14	75.00
CN	<i>CD</i>	0.55	0.72	0.69	0.65	0.54
	<i>GY</i>	0.55	0.65	0.63	0.58	0.54
DNR	<i>CD</i>	0.94	0.73	0.84	0.81	0.75
	<i>GY</i>	0.91	0.76	0.85	0.86	0.75
URETHRA						
$V_{125,ur}(\%)$	<i>CD</i>	80.56	72.97	68.75	16.13	100.00
	<i>GY</i>	66.67	81.08	75.00	87.10	100.00
$V_{360,ur}(\%)$	<i>CD</i>	0.00	0.00	0.00	0.00	0.00
	<i>GY</i>	0.00	0.00	0.00	0.00	0.00
$D_{90,ur}(\text{Gy})$	<i>CD</i>	176.50	179.37	172.41	155.27	212.75
	<i>GY</i>	163.91	179.65	173.92	179.76	212.75
RECTUM						
$V_{80,re}(\%)$	<i>CD</i>	59.73	38.02	38.39	9.90	11.71
	<i>GY</i>	60.40	52.07	23.21	14.85	11.71
$V_{90,re}(\%)$	<i>CD</i>	89.26	97.52	97.32	78.22	39.64
	<i>GY</i>	91.95	100.00	95.54	78.22	39.64
$D_{90,re}(\text{Gy})$	<i>CD</i>	90.40	98.11	98.38	83.66	57.20
	<i>GY</i>	92.01	103.74	95.26	84.83	57.20
NORMAL TISSUE						
$D_{90,no}(\text{Gy})$	<i>CD</i>	31.90	46.15	51.34	37.37	13.89
	<i>GY</i>	31.28	51.17	62.35	47.46	13.89
QUALITATIVE						
<i>Seeds</i>	<i>CD</i>	15	20	24	17	7
	<i>GY</i>	15	22	26	20	7

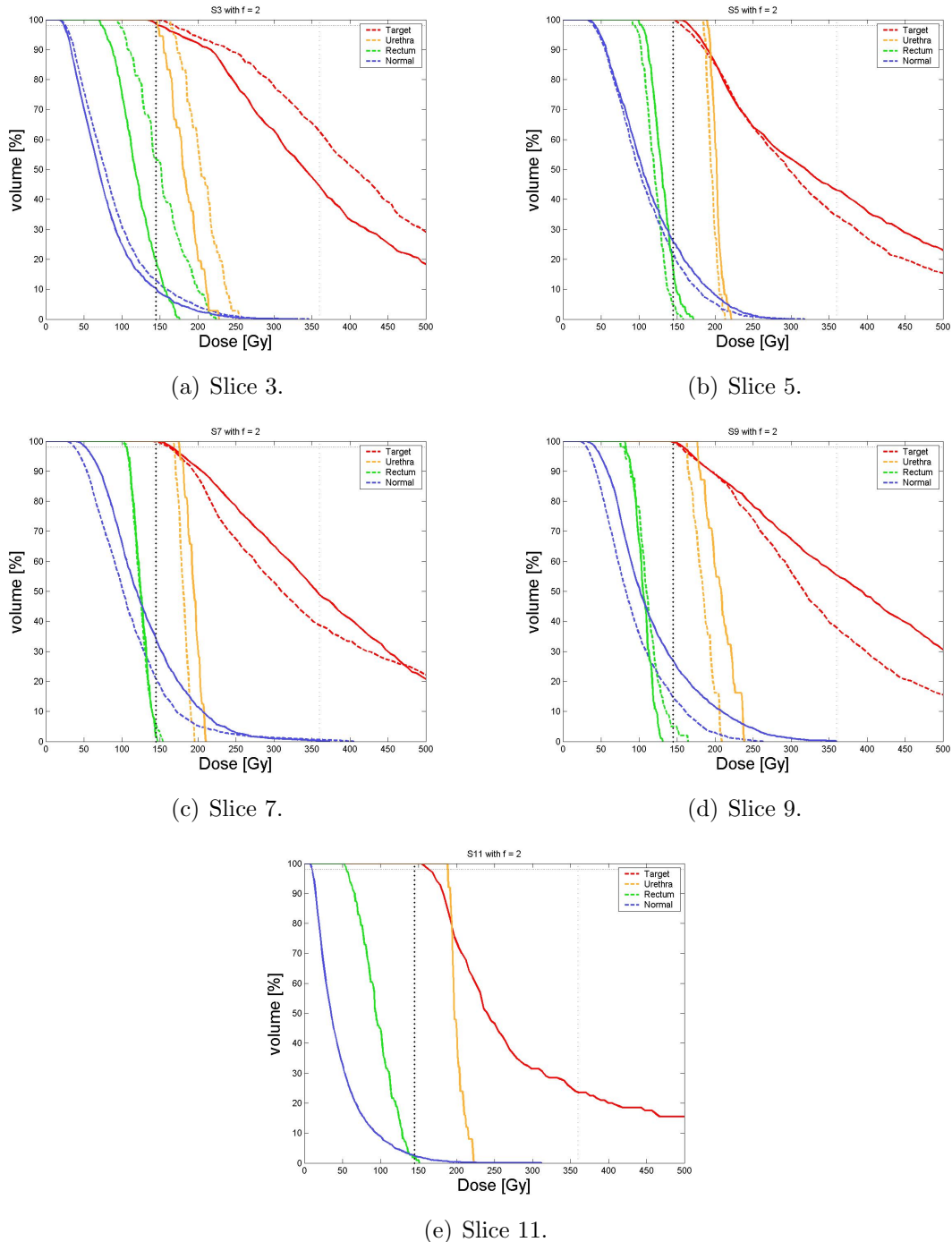
Table 5.1: CD: Evaluation parameters for $f = 1$, with grid.

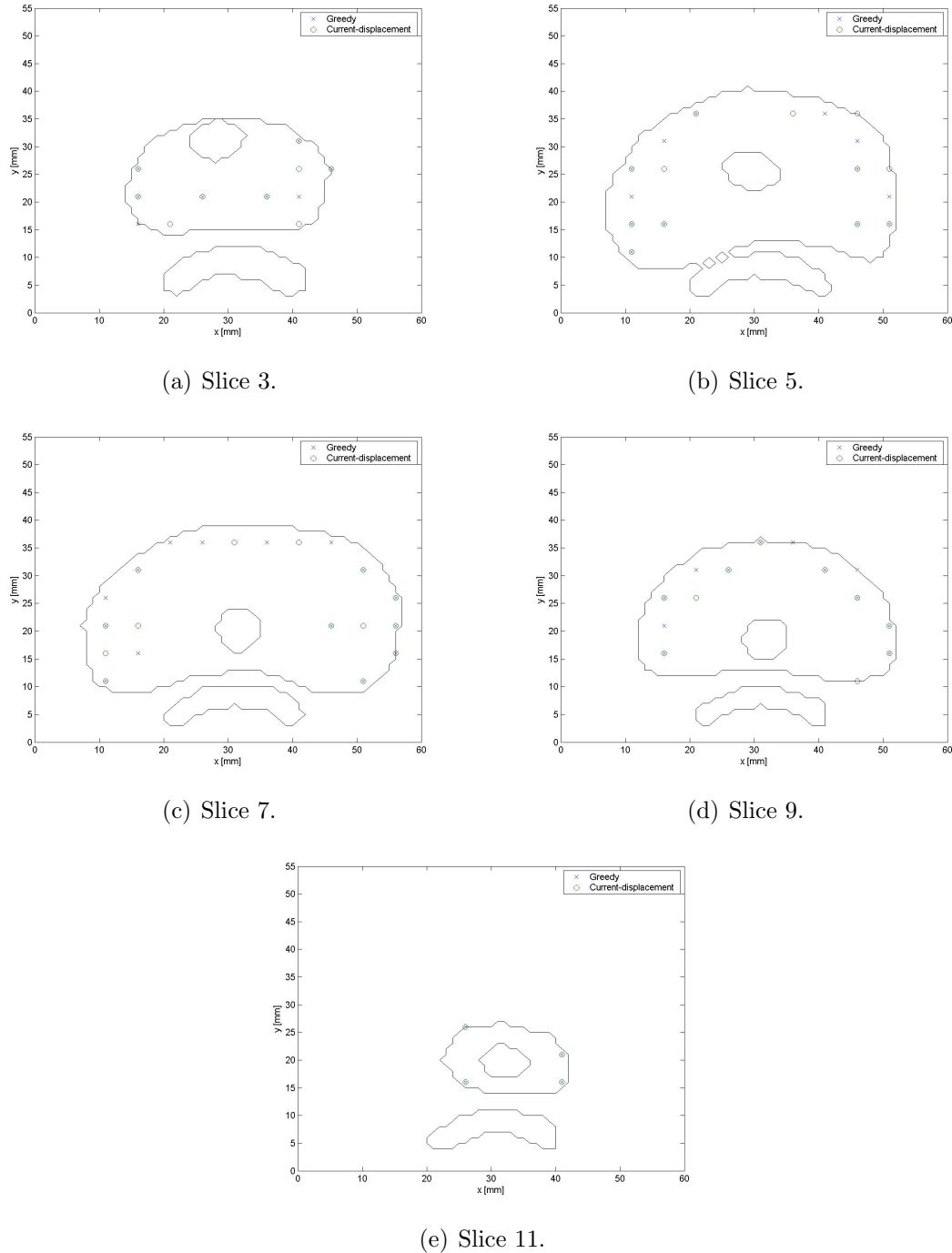
Figure 5.1: CD: DVH's for each slice with $f = 1$, with grid.

Figure 5.2: DVH's for each slice with $f = 1$, with grid.

		S3	S5	S7	S9	S11
TARGET						
$V_{100}(\%)$	<i>CD</i>	100.00	99.65	99.68	99.28	100.00
	<i>GY</i>	98.16	100.00	100.00	99.76	100.00
$V_{150}(\%)$	<i>CD</i>	91.91	77.23	78.31	83.63	62.00
	<i>GY</i>	89.89	74.55	86.13	84.83	62.00
CN	<i>CD</i>	0.45	0.60	0.63	0.56	0.47
	<i>GY</i>	0.50	0.59	0.56	0.49	0.47
DNR	<i>CD</i>	0.92	0.77	0.79	0.84	0.62
	<i>GY</i>	0.92	0.75	0.86	0.85	0.62
URETHRA						
$V_{125,ur}(\%)$	<i>CD</i>	83.33	100.00	46.88	54.84	100.00
	<i>GY</i>	50.00	100.00	84.38	87.10	100.00
$V_{360,ur}(\%)$	<i>CD</i>	0.00	0.00	0.00	0.00	0.00
	<i>GY</i>	0.00	0.00	0.00	0.00	0.00
$D_{90,ur}(\text{Gy})$	<i>CD</i>	173.42	188.78	171.15	166.17	192.75
	<i>GY</i>	155.21	194.83	182.13	181.43	192.75
RECTUM						
$V_{80,re}(\%)$	<i>CD</i>	82.55	57.02	72.32	35.64	21.62
	<i>GY</i>	51.68	83.47	75.89	24.75	21.62
$V_{90,re}(\%)$	<i>CD</i>	100.00	100.00	100.00	88.12	59.46
	<i>GY</i>	87.92	100.00	100.00	90.10	59.46
$D_{90,re}(\text{Gy})$	<i>CD</i>	108.03	103.72	111.81	89.14	66.89
	<i>GY</i>	87.49	112.60	111.33	91.31	66.89
NORMAL TISSUE						
$D_{90,no}(\text{Gy})$	<i>CD</i>	37.95	55.48	54.47	43.33	15.55
	<i>GY</i>	34.12	57.98	72.60	59.11	15.55
QUALITATIVE						
<i>Seeds</i>	<i>CD</i>	9	12	14	10	4
	<i>GY</i>	8	13	15	12	4

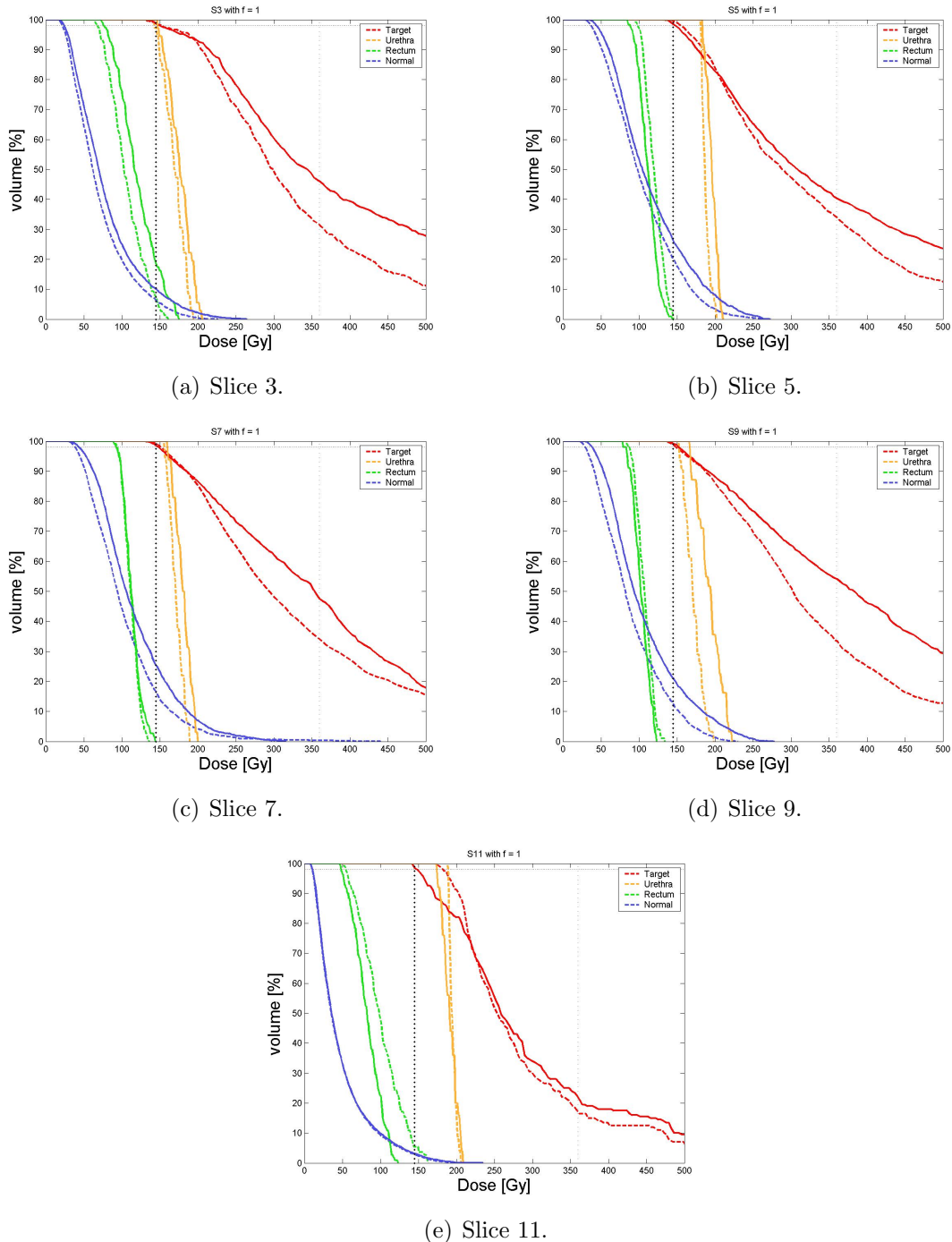
Table 5.2: CD: Evaluation parameters for $f = 2$, with grid.

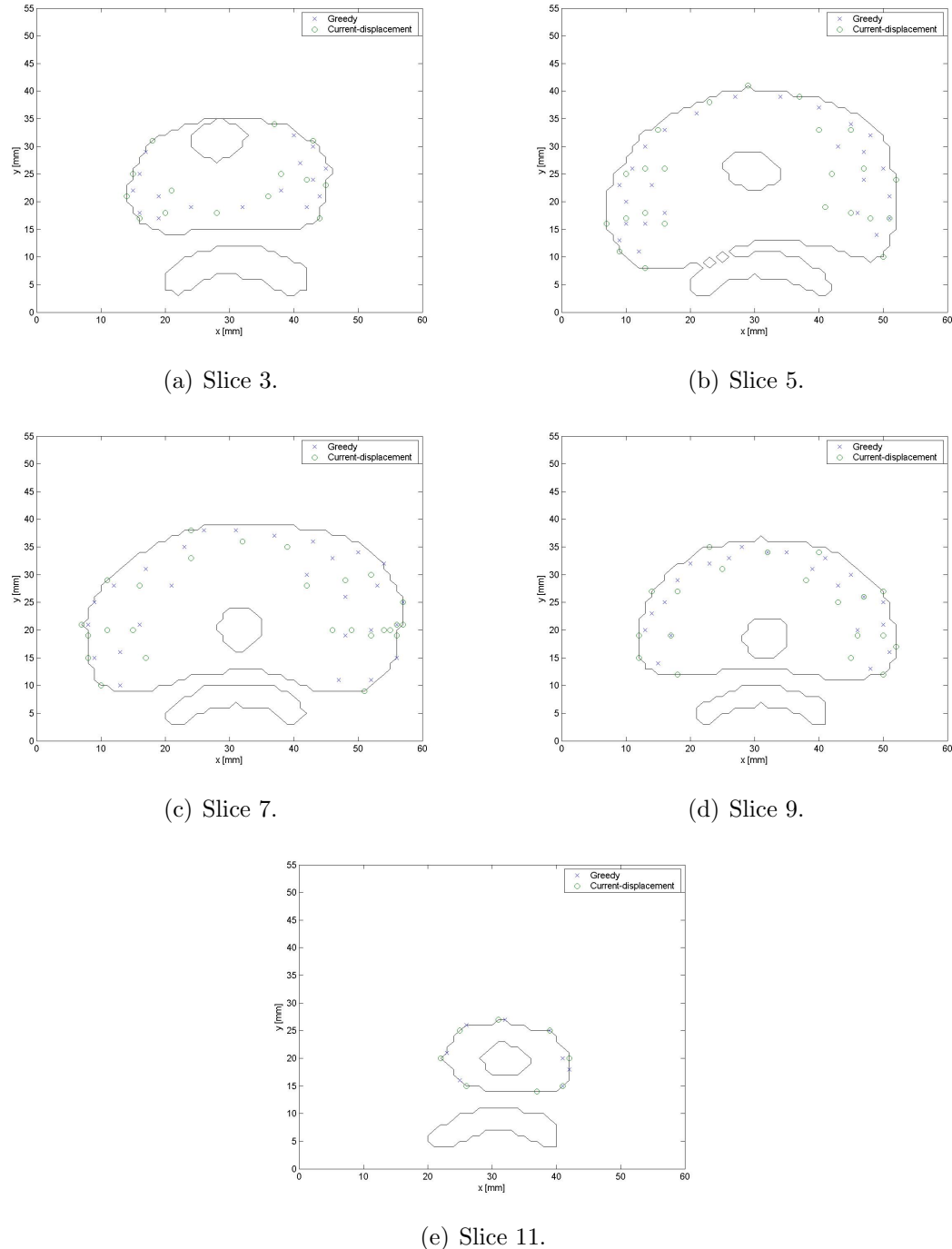
Figure 5.3: DVH's for each slice with $f = 2$, with grid.

Figure 5.4: Seed placements, $f = 2$, with grid.

		S3	S5	S7	S9	S11
TARGET						
$V_{100}(\%)$	<i>CD</i>	98.35	99.39	98.47	98.45	100.00
	<i>GY</i>	98.35	98.27	98.06	98.92	98.50
$V_{150}(\%)$	<i>CD</i>	84.74	73.94	77.66	79.93	74.50
	<i>GY</i>	88.42	75.76	81.29	83.51	72.00
CN	<i>CD</i>	0.56	0.62	0.63	0.57	0.42
	<i>GY</i>	0.50	0.59	0.60	0.53	0.43
DNR	<i>CD</i>	0.86	0.74	0.79	0.81	0.75
	<i>GY</i>	0.90	0.77	0.83	0.84	0.73
URETHRA						
$V_{125,ur}(\%)$	<i>CD</i>	22.22	89.19	21.88	25.81	100.00
	<i>GY</i>	41.67	100.00	50.00	70.97	76.00
$V_{360,ur}(\%)$	<i>CD</i>	0.00	0.00	0.00	0.00	0.00
	<i>GY</i>	0.00	0.00	0.00	0.00	0.00
$D_{90,ur}(\text{Gy})$	<i>CD</i>	149.52	182.16	159.93	158.83	190.47
	<i>GY</i>	154.40	186.18	166.15	169.37	178.66
RECTUM						
$V_{80,re}(\%)$	<i>CD</i>	31.54	57.02	33.04	23.76	27.93
	<i>GY</i>	49.66	38.02	37.50	12.87	2.70
$V_{90,re}(\%)$	<i>CD</i>	72.48	100.00	100.00	95.05	61.26
	<i>GY</i>	85.91	96.69	99.11	86.14	36.04
$D_{90,re}(\text{Gy})$	<i>CD</i>	77.47	105.42	99.37	94.04	64.64
	<i>GY</i>	88.80	96.48	99.60	89.30	58.19
NORMAL TISSUE						
$D_{90,no}(\text{Gy})$	<i>CD</i>	31.56	51.53	52.71	41.20	15.79
	<i>GY</i>	34.19	61.15	62.88	53.94	16.38
QUALITATIVE						
<i>Seeds</i>	<i>CD</i>	14	23	26	19	8
	<i>GY</i>	16	25	27	22	8

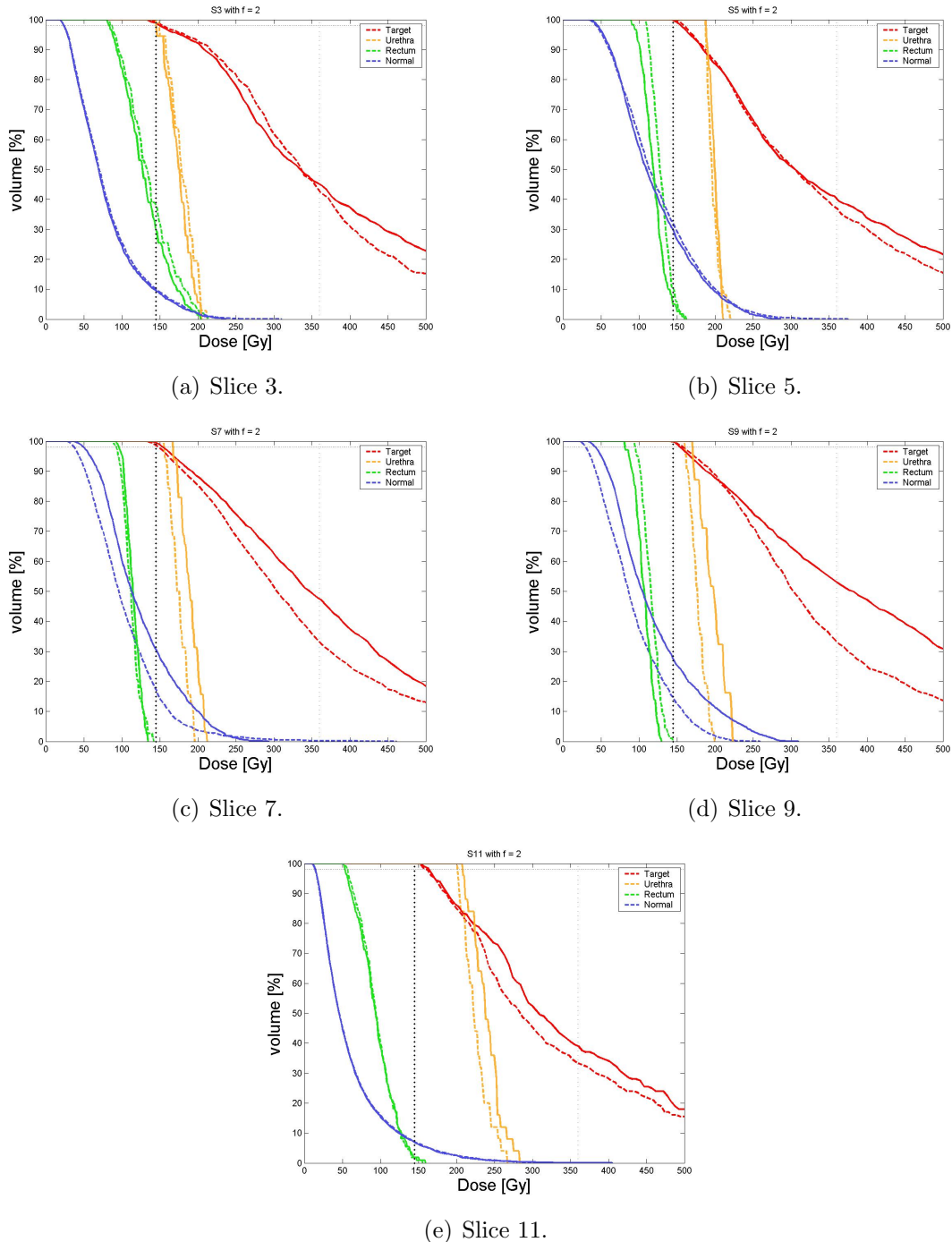
Table 5.3: CD: Evaluation parameters for $f = 1$, without grid.

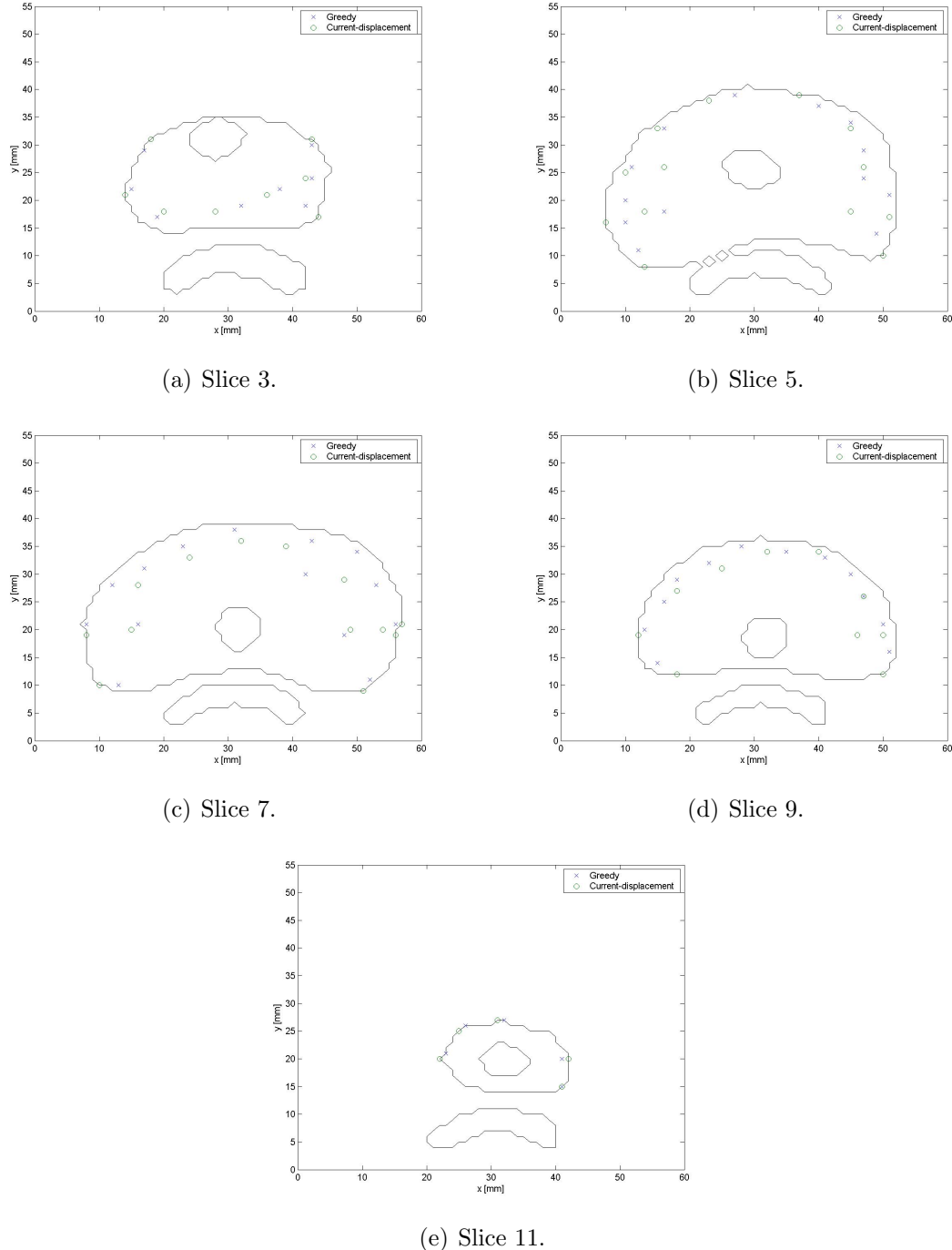
Figure 5.5: DVH's for each slice with $f = 1$, without grid.

Figure 5.6: Seed placements, $f = 1$, without grid.

		S3	S5	S7	S9	S11
TARGET						
$V_{100}(\%)$	<i>CD</i>	98.90	99.91	98.06	99.52	100.00
	<i>GY</i>	98.35	99.31	99.19	99.28	100.00
$V_{150}(\%)$	<i>CD</i>	89.52	77.84	80.24	82.80	77.50
	<i>GY</i>	87.87	78.79	83.79	82.92	81.00
CN	<i>CD</i>	0.49	0.57	0.63	0.55	0.35
	<i>GY</i>	0.51	0.58	0.58	0.48	0.35
DNR	<i>CD</i>	0.91	0.78	0.82	0.83	0.78
	<i>GY</i>	0.89	0.79	0.84	0.84	0.81
URETHRA						
$V_{125,ur}(\%)$	<i>CD</i>	44.44	100.00	31.25	35.48	100.00
	<i>GY</i>	36.11	100.00	68.75	74.19	100.00
$V_{360,ur}(\%)$	<i>CD</i>	0.00	0.00	0.00	0.00	0.00
	<i>GY</i>	0.00	0.00	0.00	0.00	0.00
$D_{90,ur}(\text{Gy})$	<i>CD</i>	158.36	189.41	160.79	165.51	204.55
	<i>GY</i>	155.56	190.80	173.17	173.36	211.59
RECTUM						
$V_{80,re}(\%)$	<i>CD</i>	67.79	81.82	34.82	46.53	19.82
	<i>GY</i>	63.09	57.02	44.64	21.78	20.72
$V_{90,re}(\%)$	<i>CD</i>	95.30	100.00	99.11	100.00	56.76
	<i>GY</i>	93.29	98.35	100.00	91.09	54.95
$D_{90,re}(\text{Gy})$	<i>CD</i>	95.66	113.76	98.87	102.25	65.77
	<i>GY</i>	93.22	101.70	102.84	91.71	62.56
NORMAL TISSUE						
$D_{90,no}(\text{Gy})$	<i>CD</i>	34.00	61.70	52.84	43.91	20.52
	<i>GY</i>	34.20	62.77	70.19	60.20	22.21
QUALITATIVE						
<i>Seeds</i>	<i>CD</i>	8	13	13	10	5
	<i>GY</i>	8	13	14	12	5

Table 5.4: CD: Evaluation parameters for $f = 2$, without grid.

Figure 5.7: DVH's for each slice with $f = 2$, without grid.

Figure 5.8: Seed placements, $f = 2$, without grid.

1.7%.

Similarly, the CN and DNR values achieved by CD are better than those for GY. Of the twenty cases, CD generated higher CN and lower DNR values for 13 cases. On average, CN was increased by 5% and DNR was decreased by 1.8%.

Overall, CD improves the quality of target irradiation.

Urethra Sparing

In no case does the urethra receive greater than 360 Gy. Furthermore, note that $V_{125,ur}$ is lower for CD in 11 of 20 cases; on average, $V_{125,ur}$ is 16.5% lower for CD, a marked improvement. $D_{90,ur}$ is also reduced for CD in 14 cases for an average reduction of 1.9% or about 3 Gy. Thus, CD yields a significantly better plan with respect to urethra sparing.

Rectum Sparing

From Tables 5.1-5.4, we see on average that CD leads to higher $V_{90,re}$ by about 2.7% and showed improvement on just four cases. Additionally, $V_{80,re}$ is significantly higher for CD, especially for the cases without the treatment grid. For these cases, $V_{80,re}$ rises by about 22%; for the cases with the treatment grid, this increase is just 0.9%, meaning CD leads to an average increase in $V_{80,re}$ of 10.9%. Additionally, CD raises $D_{90,re}$ by 2.1%. Thus, CD gives rise to diminished rectum sparing.

Normal Tissue Sparing

CD generated better or equivalent normal tissue sparing for all but two cases. GY led to an average $D_{90,no}$ of 46.2 Gy whereas CD had an average $D_{90,no}$ of 39.7 Gy, a significant 14.1% decrease in normal tissue dose.

Number of Seeds

As mentioned above, reducing the number of seeds used in a treatment plan helps both to prevent possible over-dosing and to provide as economical a plan as possible. In only one case ($f = 2$, slice 3, with grid) does the CD generate a plan using more seeds, and consequently, the CD DVH curves are seen to be significantly worse. In 12 cases, CD uses fewer seeds, and in the remaining 7 cases, CD and GY use the same number of seeds. On average, CD uses one fewer seed than GY, a 7.2% reduction.

General Remarks

Overall, CD-driven greedy heuristic leads to better target coverage and improved sparing of the urethra and surrounding normal tissues. Additionally, CD uses fewer seeds on average. However, rectum sparing was worse for CD, and further work should be done to produce better rectum sparing. Even so, the use of the normed current-displacement as the greedy criterion does seem warranted, and further work in three-dimensions should be explored.

CHAPTER 6

CONCLUDING REMARKS

This work has described two novel approaches that employ ROI adjoint current vectors in brachytherapy treatment planning for prostate cancer. The adjoint current measures both the direction and magnitude of the net flow of the “importance” a seed at any position has on the dose to the ROI.

The first approach uses these current vectors to define the so-called *current-displacement*, which quantifies the “force” exerted on a seed at some position. The force on all seeds is translated into an appropriate displacement vector used to find new seed positions. The adjoint function-driven greedy heuristic is used to generate initial seed placements from which new seed positions are found. The new method applying current-displacement was compared to the original greedy heuristic and was found to improve many of the dosimetric quantities studied, with urethral quantities being most improved.

The second approach uses the L_2 norm of a modified current-displacement as a new greedy criterion for use in the greedy heuristic. This method was compared to the original greedy heuristic and was found to improve substantially target irradiation and sparing of the urethra and normal tissues. However, increased dose to the rectum was an issue and warrants further improvement. Additionally, the new method used fewer seeds on average than the original greedy heuristic.

Both uses of adjoint current showed improvement over established methods. Thus, it seems further applications of the adjoint current could also be useful. Chaswal in [2] looks at ways to use the adjoint concept in placement of directional seeds. While the statistical-based approach does yield good results, it seems that adjoint angular information, e.g. the adjoint current, contains exactly that information needed in placing directional seeds. Currently, research in that area is being conducted and will constitute one portion of the next step in this work.

To aid in this and similar research, more work should be done to quantify and qualify the evaluation parameters reviewed above. While the parameters certainly facilitate comparison of treatment plans, knowing *a priori* which criterion (or criteria) are most important to a “good” treatment plan would be a great benefit. Here, the idea was simply to “make as many better as possible.”

As has been discussed in this report, there are limitations to working in two-dimensions. Additionally, the underlying theory to the methods of Chapter 5 do not have any groundings in the biology of the problem. Perhaps moving toward incorporating a deeper biological connection, e.g. via using tissue volumes as a starting point, could help improve the rectum quantities observed. However, the full extent of the success or shortcomings of the two methods described here will only be known upon translation to three-dimensions. It is hoped the methods used throughout are easily adaptable to three-dimensions and furthermore that the same improvements seen here are realized in future work.

APPENDIX A

SCALAR FLUX UTILITY

The following provides a listing of code used to read and print the DANTSYS scalar flux file.

```
program scalflx

!-----
! This program reads the scalar flux file from the TWODANT neutronics !
! program. The files read are either RTFLUX or ATFLUX, representing !
! the forward and adjoint case, respectively. !
! j.roberts feb 10 08 !
!-----

! command line format:
!   ./scalflx <prefix> <0 or 1> <a or b>
! where
!   0 = forward file, i.e. RTFLUX
!   1 = adjoint file, i.e. ATFLUX
! and
!   a = format type one, i.e. <group i j flux>
!   b = format type two, i.e. [flux_ij] for each group

implicit none

!--- variable declarations ---!
integer, parameter :: dp = selected_real_kind(10)
integer :: cl_count, cl_length, uin, uot, iver, &
```

```

        ndim, ngrp, ninti, nintj, nintk, nblok,  openStat, &
        jup, ju, jl
integer :: ii, jj, kk, i, j, k, l, g, m
character(12) :: prefix, output
real (kind = dp), dimension(150,160) :: freg
real (kind = dp), dimension(3,150,160) :: phi
integer, dimension(7) :: ispec
real, dimension(2) :: spec
character :: hname*6, huse(2)*6, aint*3, scorad*1, prtype*1

cl_count = command_argument_count()
if ( cl_count /= 3 ) then
    print *, "Command Line Error"
    print *, "Format ./scalflx <prefix> <0 or 1> <a or b>"
    print *, " which is then used to produce:"
    print *, " <prefix>.sclflx"
    stop
end if

!-- assign variables from command line --
call get_command_argument ( 1, prefix, cl_length )
output(1:cl_length) = prefix
output(cl_length+1:cl_length+5) = ".out"
call get_command_argument ( 2, scorad)
call get_command_argument ( 3, prtype)
print *, 'output is', output
if ( scorad == '0' ) then
    print *, "Reading RTFLUX file..."
else if ( scorad == '1' ) then
    print *, "Reading ATFLUX file..."
else
    stop "*** second var not 0/1 for forward/adjoint ***"
end if

uin = 2 ! input unit
uot = 6 ! output unit

if (scorad == '0') then
    open(unit=uin, file='rtflux', status='old', &
          form='unformatted', position = 'rewind', &
          iostat = openStat)
    if (openStat > 0) stop "*** RTFLUX not found ***"

```

```

else
    open(unit=uin,file='atflux',status='old', &
          form='unformatted', position = 'rewind', &
          iostat = openStat)
    if (openStat > 0) stop "*** ATFLUX not found ***"
end if

open (unit=uot, file=output, action="write", &
      form='formatted', status = "unknown", &
      iostat = openStat)
if (openStat > 0) stop "*** output file handling error ***"

!-- begin reading --!

read(uin) hname,(huse(i),i=1,2),iver
print *, hname,(huse(i),i=1,2),iver
! one could print this stuff, but it's rather irrelevant
! for the problem at hand

read(uin) (ispec(i),i=1,6), spec(1), spec(2), ispec(7)
print *, (ispec(i),i=1,6), spec(1), spec(2), ispec(7)

ndim = ispec(1)
ngrp = ispec(2)
ninti = ispec(3)
nintj = ispec(4)
nintk = ispec(5)
nblok = ispec(7)

do l = 1, ngrp
    do k = 1, nintk
        do m = 1, nblok
            jl = (m-1) * ((nintj-1) / nblok + 1) + 1
            jup = m * ((nintj-1) / nblok + 1)
            ju = min( nintj , jup )
            read(uin) ((freq(i,j),i=1,ninti),j=jl,ju)
            !write(uot,115) ((freq(i,j),i=1,ninti),j=1,5)
            do jj=jl,ju
                do ii = 1,ninti
                    phi(l,ii,jj) = freq(ii,jj)
                    write(uot,117) l, ii, jj, freq(ii,jj)
            end do
        end do
    end do
end do

```

```
        end do
    end do
end do

print *, "...done"

110 format(5x,'group = ',i4)
115 format(6(3x,e9.3))
116 format(150(2x,e9.3))           ! phi matrix
117 format(5x,i4,5x,i4,5x,i4,5x,e9.3) ! (group,i,j,phi)

end program scalflx
```

APPENDIX B

CURRENT VECTOR UTILITY

The following provides a listing of code used to read the DANTSYS angular flux file and print the cell-centered current vector. This code is based on ones from M. Seydaliev.

```
program curcalc

!-----
! This program reads the adjoint flux file from the TWODANT neutronics!
! program. The files read are either RAFLXM or AAFLXM, representing !
! the forward and adjoint case, respectively. The output is the x and !
! y component of the cell-centered current vector !
! j.roberts feb 15 08 !
! based on code by m. seydaliev !
!-----

implicit none

! command line format:
! ./angflx <prefix> <0 or 1> <anything>
! where
!   0 = forward file, i.e. RAFLXM
!   1 = adjoint file, i.e. AAFLXM
! and
!   output = cell-centered current printed, [g i j cur_x cur_y]

!-- variable declarations --!

integer :: cl_count, cl_length, uin, uou, ndim, ngroup, &
           ninti, nintj, nintk, nblok, openStat, iver, &
```

```

          ith, i, j, k, g, l, d, m, ndir
double precision :: power, effk, xm, xeta, weight, xm
double precision :: angflux
character(12) :: prefix, output
double precision, dimension(1500,1600) :: ahedge, &
     avedge,hcntrb, vcntrb, angfluxh, angfluxv
double precision, dimension(3,1500,1600) :: curx, cury
integer, dimension(6) :: ispec
real, dimension(2) :: spec
integer, dimension(3) :: nspec
character :: hname*6, huse(2)*6, scorad*1, prtype*1
double precision, dimension(4) :: cosi

!-- file handling --!

cl_count = command_argument_count()
if ( cl_count /= 3 ) then
    print *, "Command Line Error"
    print *, "Format ./scalflx <prefix> <0 or 1> <a or b>"
    print *, " which is then used to produce:"
    print *, " <prefix>.sclf"
    stop
end if

!-- assign variables from command line --
call get_command_argument ( 1, prefix, cl_length )
output(1:cl_length) = prefix
output(cl_length+1:cl_length+5) = ".cur"
call get_command_argument ( 2, scorad)
call get_command_argument ( 3, prtype)
print *, 'output is ', output
if ( scorad == '0' ) then
    ith = 1
    print *, "Reading RAFLXM file..."
else if ( scorad == '1' ) then
    ith = -1
    print *, "Reading AAFLXM file..."
else
    stop "*** second var not 0/1 for forward/adjoint ***"
end if

uin = 2 ! input unit

```

```

uou = 6 ! output unit

if (scorad == '0') then
    open(unit=uin, file='raflxm', status='old', &
         form='unformatted', position = 'rewind', &
         iostat = openStat)
    if (openStat > 0) stop "*** RAFLXM not found ***"
else
    open(unit=uin,file='aaflxm',status='old', &
         form='unformatted', position = 'rewind', &
         iostat = openStat)
    if (openStat > 0) stop "*** AAFLXM not found ***"
end if

open (unit=uou, file=output, action="write", form='formatted', &
      status = "unknown", iostat = openStat)
if (openStat > 0) stop "*** output file handling error ***"

!-- file reading begins --!

read(uin) hname,(huse(i),i=1,2),iver
print *, hname,(huse(i),i=1,2),iver
read(uin) (ispec(i),i=1,6), spec(1), spec(2)
print *, (ispec(i),i=1,6), spec(1), spec(2)

ndim = ispec(1)
ngroup = ispec(2)
ninti = ispec(3)
nintj = ispec(4)
nintk = ispec(5)
ndir = ispec(6)
effk = spec(1)
power = spec(2)

!-- read angular fluxes --!

do l=1,ngroup
    do d=1,ndir

        read(uin) (cosi(m),m=1,4)
        xmu=cosi(1)

```

```

xeta=cosi(2)
weight=cosi(3)
xm=cosi(4)

read(uin) ((ahedge(i,j),i=1,ninti+1),j=1,nintj)
read(uin) ((avedge(i,j),i=1,ninti),j=1,nintj+1)

do j=1,nintj
    do i=1,ninti
        angfluxh(i,j)=(ahedge(i,j)+ahedge(i+1,j))/2.
        angfluxv(i,j)=(avedge(i,j)+avedge(i,j+1))/2.
        angflux = (angfluxh(i,j)+angfluxv(i,j))/2.
        curX(l,i,j) = curX(l,i,j) - angflux*xmu*weight
        curY(l,i,j) = curY(l,i,j) - angflux*xeta*weight
    end do
end do

end do
end do

do l=1,ngroup
    do j=1,nintj
        do i=1,ninti
            write(uou,121) l,i,j, curX(l,i,j),curY(l,i,j)
        end do
    end do
end do

106 format(5x,'mu    = ',e9.3,/,&
           5x,'eta   = ',e9.3,/ &
           5x,'weight= ',e9.3)
109 format(5x,'direction= ',e9.3)
110 format(5x,'group = ',i4)
115 format(10(3x,e9.3))
118 format(5x,'mesh point = ', i6)
119 format(1x,e9.3,13x,e9.3,10x,i5,i5)
121 format(1x, i5, i5, i5, 5x, e9.3, 5x, e9.3)

end program curcalc

```

APPENDIX C

DANTSYS INPUT EXAMPLE

The following provides a listing of the DANTSYS input for generation of target adjoint data for slice 9.

```
      3      0      0
Patient Data - Target, slice 9
USING 3-GROUP CROSS SECTION LIBRARY
Calculate Adjoint flux, Current For Optimization
/ geometry      - 2-d region of 'tissue'
/ cross section - 3 group / limited elements
/
/ ----- Block 1 (Control and Dimensions) -----
  igeom= x-y  ngroup= 3  isn= 8  niso= 39  mt= 1
          nzone= 1    im= 6    it= 60   jm= 6   jt= 55
  maxlcm= 800000
  maxscm= 1250000
  idimen= 2
  t
/
/ ----- Block 2 (Geometry) -----
/ 1cm x 1cm region
/
  xmesh= 0.0  1.0  2.0  3.0  4.0  5.0  6.0
  xints=     10    10    10    10    10    10
  ymesh= 0.0  1.0  2.0  3.0  4.0  5.0  5.5
  yints=     10    10    10    10    10     5
```

```

zones=    1      1      1      1      1      1 ;  

          1      1      1      1      1      1 ;  

          1      1      1      1      1      1 ;  

          1      1      1      1      1      1 ;  

          1      1      1      1      1      1 ;  

          1      1      1      1      1      1 ;  

          1      1      1      1      1      1 ;  

          t  

/  

/ ----- Block 3 (Cross Section) -----  

/  

lib= xslib  

lng= 0  

maxord= 5 ihm= 11 iht= 8 ihs= 9 ifido= 1 ititl= 1  

        i2lp1= 1 savbxs= 0 kwikrd= 0  

t  

/  

/ ----- Block 4 (Material Mixing) -----  

/  

matls=  

        wtr   1 6.6666-2 12 3.3333-2;  

assign=  

        prostate wtr 1.00 ;  

t  

/  

/ ----- Block 5 (Solver) -----  

/  

ievt= 0 isct= 1 ith= 1 ibl= 0 ibr= 0 iitl= 300 iquad= 1  

fluxp= 0 xsectp= 0 fissrp= 0 sourcp= 0 geomp= 1  

        angp= 0 raflux= 0 rmflux= 0 balp= 1  

norm=0  

/  

/ ----- Source Input -----  

/ source- left bdry source input per incoming quadrature angle  

fcsrc= ray fcntr= 25  

source= 2.78e-7 1.11e-6 4.22e-7  

sourcf=  

        60z ;  

        60z ;  

        60z ;  

        60z ;  

        60z ;  

        60z ;

```

```
60z ;
60z ;
60z ;
60z ;
40z 7r 1 13z ;
14z 10r 1 11z 15r 1 10z ;
12z 39r 1 9z ;
12z 39r 1 9z ;
11z 41r 1 8z ;
11z 18r 1 4z 19r 1 8z ;
11z 18r 1 5z 18r 1 8z ;
11z 17r 1 6z 18r 1 8z ;
11z 17r 1 6z 18r 1 8z ;
11z 18r 1 5z 18r 1 8z ;
11z 18r 1 5z 18r 1 8z ;
11z 40r 1 9z ;
12z 39r 1 9z ;
12z 39r 1 9z ;
12z 39r 1 9z ;
13z 37r 1 10z ;
13z 37r 1 10z ;
14z 35r 1 11z ;
15z 33r 1 12z ;
15z 32r 1 13z ;
16z 30r 1 14z ;
17z 28r 1 15z ;
19z 25r 1 16z ;
20z 23r 1 17z ;
21z 20r 1 19z ;
25z 13r 1 22z ;
30z 1r 1 29z ;
60z ;
```

```
60z ;  
t
```

REFERENCES

- [1] G. I. Bell and S. Glasstone. *Nuclear Reactor Theory*. Van Nostrand Reinhold, 1970.
- [2] V Chaswal. *Adjoint Based Treatment Planning for Brachytherapy: Novel Techniques and Further Developments*. PhD thesis, University of Wisconsin - Madison, 2008.
- [3] V Chaswal, S Yoo, B R Thomadsen, and D L Henderson. Investigations into the use of multi-species seeds in interstitial prostate implant brachytherapy using the 3-D treatment optimization program based upon the region of interest adjoint functions and greedy heuristic algorithm. *Medical Physics*, 31(6):1746, JUN 2004.
- [4] V Chaswal, S Yoo, B R Thomadsen, and D L Henderson. Multi-species prostate implant treatment plans incorporating Ir-192 and I-125 using a Greedy Heuristic based 3D optimization algorithm. *Medical Physics*, 34(2):436–444, FEB 2007.
- [5] T. H. Cormen, C. E. Leiserson, R. L. Rivest, and C. Stein. *Introduction to Algorithms*. MIT Press, 1995.
- [6] DANTSYS. *User's Guide*. LA-12969-M(Los Alamos: The Applied Physics (X) Division of Los Alamos National Laboratory, 1997.
- [7] ICRP Committee 3 Task Group, P Grande, and M. C. O'riordant, chairman. Data for Protection Against Ionizing Radiation from External Sources: Supplement to ICRP Publication 15. Technical report, International Commission of Radiological Protection, APR 1971.
- [8] D. L. Henderson, S. Yoo, M. Kowalok, T. R. Mackie, and B. R. Thomadsen. The Adjoint Method for The Optimization of Brachytherapy and Radiotherapy Patient Treatment Planning Procedures Using Monte Carlo Calculations. Technical report, DOE/ID/13774, University of Wisconsin-Madison (US), 2001.
- [9] E. E. Lewis and W. F. Miller. *Computational Methods of Neutron Transport*. American Nuclear Society, 1984.
- [10] S. Nag, D. Beyer, J. Friedland, P. Grimm, and R. Nath. American Brachytherapy Society (ABS) recommendations for transperineal permanent brachytherapy of prostate cancer. *Int J Radiat Oncol Biol Phys*, 44(4):789–99, 1999.

- [11] R. Nath, L.L. Anderson, G. Luxton, K.A. Weaver, J.F. Williamson, and A.S. Meigooni. Dosimetry of interstitial brachytherapy sources: Recommendations of the AAPM Radiation Therapy Committee Task Group No. 43. *Medical Physics*, 22:209, 1995.
- [12] R. Nath, L.L. Anderson, J.A. Meli, A.J. Olch, J.A. Stitt, and J.F. Williamson. Code of practice for brachytherapy physics: Report of the AAPM Radiation Therapy Committee Task Group No. 56. *Medical Physics*, 24:1557, 1997.
- [13] S. Yoo, M. Kowalok, D. Henderson, and B. Thomadsen. Seed- and needle- optimization for brachytherapy using greedy heuristic and adjoint functions. *Medical Physics*, 30(6):1429–1430, JUN 2003.
- [14] Sua Yoo, Michael E. Kowalok, Bruce R. Thomadsen, and Douglass L. Henderson. Treatment planning for prostate brachytherapy using region of interest adjoint functions and a greedy heuristic. *Physics in Medicine and Biology*, 48(24):4077–4090, DEC 21 2003.
- [15] Y. Yu, L. L. Anderson, Z. Li, D. E. Mellenberg, R. Nath, M. C. Schell, F. M. Waterman, A. Wu, and J. C. Blasko. Permanent prostate seed implant brachytherapy: Report of the American Association of Physicists in Medicine Task Group No. 64. *Medical Physics*, 26:2054, 1999.

BIOGRAPHICAL SKETCH

Jeremy A. Roberts is currently a first year graduate student at the University of Wisconsin-Madison. Born in 1984 in the Upper Peninsula of Michigan, he moved to and then lived in the greater Green Bay area for nearly two decades. He began his studies at UW-Madison as a nuclear engineering undergraduate in 2003; he will finish his M.S. in nuclear engineering there on an AFCI/GNEP fellowship. Outside of his studies, Jeremy enjoys reading, cycling, cooking, and maintaining an otherwise simple existence.

Jeremy currently lives with his soon-to-be fiancé Samantha in west Madison, WI.